Fuel Processing Technology 222 (2021) 106940

Contents lists available at ScienceDirect

Fuel Processing Technology

journal homepage: www.elsevier.com/locate/fuproc

Review

A state-of-the-art review of lab-scale inverse diffusion burners & flames: From laminar to turbulent

H.S. Zhen [a], Z.L. Wei [a], X.Y. Liu [a], Z.H. Liu [a,*], X.C. Wang [b], Z.H. Huang [b], C.W. Leung [c]

[a] The Mechanical and Electrical Engineering College, Hainan University, Haikou, China
[b] School of Energy and Power Engineering, Xi'an Jiaotong University, Xi'an 710049, China
[c] Division of Science and Technology, College of Professional and Continuing Education, The Hong Kong Polytechnic University, Hong Kong, China

ARTICLE INFO

Keywords:
Inverse Diffusion Flame
Burner Flame
Turbulent Combustion
Young Soot

ABSTRACT

Based on the previous work, this paper presents a thorough review of the laboratory studies of IDF (inverse diffusion flame), introducing its history, its current development and foreseeing the problems to be solved in future. The review is focused on the flow and combustion behaviors during the transition of IDF from laminar to turbulent, which are well documented in the studies of IDF impingement heat transfer, and thus is aimed to provide guidance for expediting future studies of soot formation in turbulent IDF.

As a flame, IDF is influenced by the parameters of burner, fuel/oxidizer flows and chemical reactions, which can be overally classified into three types, i.e. geometrical, fluidynamic and combustion parameters. Based on these parameters, this review copes with a number of issues like IDF burner design, features of burner geometry, analysis of flow dynamics, flame structure and characters of thermal field. Firstly, the review focuses the burner geometric features, and presents a full picture of the burner design evolution in the past decades. Then, an attempt will be made to encompass the mixing mechanism between fuel and oxidizer, at either molecular or macroscopic levels. Next, an introduction is made to various flame patterns produced and their thermal and combustion characteristics. After this, the fluid mechanics and particular fluidynamic features of IDF will be fully recognized. Finally, the combustion and usages of various IDFs will be visited, gaining information of both local and global fluidynamic and thermal behaviors of IDF. Through this review work, it is intended to address the investigation need for future challenges in laboratory IDF studies as well as to put IDF into better practical applications.

1. Introduction

Inverse Diffusion Flames (IDFs) are widely used in practical applications, such as power plants [1–3], rocket engines [4–6] and gas turbines [7–9]. IDF is capable of featuring both pure diffusion and premixed flames, hence it has the advantages of both flames in terms of operational safety, flame stability and pollutant emission. With ever-growing research attention in future, IDF is expected to impact the fields of not only fuel processing, but combustion and environment pollution.

In the year of 1922, the term of 'inverse diffusion flame' was firstly presented by Friend [10] to describe reciprocal combustion: 'a flame of air burning in fuel is simply the inverse of fuel burning in air'. In consideration of reciprocal combustion, a limited amount of air ejected into a large fuel stream appears comparable to the inverse of gaseous fuel being locally injected into an excess of air. As normal combustion where a fuel is enveloped by an overall excessive oxidizer is typified by Diffusion Flame (DF) or Normal Diffusion Flame (NDF), reciprocal combustion is symbolized by inverse diffusion flame (IDF). Compared to DFs or NDFs, IDFs are capable of more premixed combustion and thus harvesting both advantages of diffusion and premixed combustion. IDFs have many implications for practical combustion devices. For an example, in furnaces with the use of air staging, primary combustion zones often have more of an IDF structure than a NDF structure [1–3].

Evoked by great interest of IDFs in practical applications, many research efforts have been made on lab-scale IDFs for fundamental study purpose. From these studies, understanding about IDF combustion, and unique features of IDFs with respect to DFs and NDFs has been advanced [6,11–18]. In the past, various types of IDF burners were designed and tested, with the flame operation and stability characteristics quantified [11,19–31]. Better knowledge of the fluidynamic, thermal, combustion

* Corresponding author.
E-mail address: ban18@126.com (Z.H. Liu).

https://doi.org/10.1016/j.fuproc.2021.106940
Received 27 March 2021; Received in revised form 24 May 2021; Accepted 9 June 2021
Available online 28 July 2021

Nomenclature

DF	Diffusion Flame
IDF	Inverse Diffusion Flame
NDF	Normal Diffusion Flame
Re	Reynolds number of fuel/air mixture jet
Re_{air}	air jet Reynolds number
Re_{fuel}	fuel jet Reynolds number
Φ	mixture equivalence ratio
Φ_o	overall or global equivalence ratio
H	nozzle to plate distance, m
d_{in}	inner diameter of inner tube, m
D_{ou}	inner diameter of outer tube, m
δ	thickness of inner tube, m
d_{air}	inner diameter of air port, m
r	radial distance from burner centerline, m

and emission behaviors of IDFs was gained [11,17,18,24,27,30–40]. The academic merit of laminar IDF was recognized that due to its particular flow features, laminar IDF was accepted as a standard flame for young soot studies and synthesis of nano-materials or functional devices [41–45]. Note that the current investigation of either soot particle formation or nano-carbon synthesis using IDFs is confined within laminar flow/flame regime [41–45]. On the other side, potential applications of turbulent IDF were sought for flame impingement heating [29,31,46–52] due to the superb premixed character of turbulent IDF. In all previous studies, IDF as well as its combustion went through diversified burners, various flow conditions and multiple physical and chemical processes. However, a review article summing up both physical and chemical features of IDFs in previous studies is hardly seen in the literature. In this regard, an extensive review of existent publications on IDFs is thirstily desired to foresee the future. This paper provides an overview of the kind mentioned. The major objective is through examination of burner geometry, fuel/air mixing and flow/flame patterns to make a full picture of both laminar and turbulent IDFs in terms of their flame and combustion characteristics. Such a full picture offers information beneficial not only to engineers to better utilise IDFs but also to researchers to conduct more in-depth studies in the future. It also inclusively benefits the future studies of soot and nano-carbon formation by extending the regime from laminar to turbulent.

The content of this review is constructed as follows. Firstly, Section 2 presents a classification of IDF burners, their historic evolution and Research & Design importance in light of fuel/air mixing for possessing combustion features of both diffusion and premixed flames. Section 3 launches an extensive survey of the fuel/air mixing field, flow/flame patterns and combustion properties of existent IDFs, giving insight into the right IDF together with its operation suitable for heating applications. Section 4 compares the fluidynamic and thermal fields of laminar IDFs and NDFs, appreciating the merits of laminar IDFs for young soot investigation. The fuel/air mixing, fluidynamic and thermal fields of turbulent IDFs are judged by aiming at extending soot or nano-material studies from laminar to turbulent IDFs. Section 5, judging from the literature reviewed, points out the scope of future work in the fundamental research field, and several suggestions are also given in this final section of the review.

2. Lab-scale IDFs

The growing relevance of IDFs in practical applications has aroused fundamental research studies to be conducted on laboratory small-scale IDF burners. For example, driven by the need for higher thermal load (higher heat transfer rate) of a single flame, IDF can be used in heating application. In such application, IDF is safer than premixed flame while cleaner than diffusion flame or normal diffusion flame. As an IDF has diversified physical and chemical characteristics, their studies are generally multi-oriented by putting different priorities on burner design, flow/flame operation, flame appearance (including shape/size/length/color), thermal temperature, flame structures and pollutant emissions. In the past, various fuels have been tested to study the nature of IDF [31,53–55]. Numerous researches were devoted to studying the effects of burner geometry and fluid dynamics on the combustion characteristics [16,19–21,30–34,51,53,55–57]. Through these research efforts, not only significant improvement in burner design has been achieved, but also greater knowledge of reacting and non-reacting flow/flame properties about IDFs is gained. Here first of all in this review, collective information is derived from previous studies to bring out classified types of IDFs, burner features and basic flow/flame structures. Table 1 is a summarized category of some typical IDFs in the previous studies.

2.1. Classification of IDF burners

Burner is the basic unit of apparatus for a flame study. Normal diffusion flame or burner is illustrated in Fig. 1a, where fuel flows in the inner tube while air flows through the outer tube. Note that if the outer tube is removed, it becomes a pure diffusion burner or flame. The burner can further change into premixed burner if the inner tube issues a fuel/air mixture. As known, DF has wider operation and thus is stable than PF, while PF is cleaner than DF.

In this review, classification of existent IDF burners is made according to their capability of achieving fuel/air mixing. Primarily, there are three basic designs of IDF burners shown in Fig. 1b~d in accordance with their capability for fuel/air mixing. The first is a coflow or coaxial (CoA) burner, simply constructed by two concentric tubes of different diameters. Air flows through the inner tube and fuel the outer tube, such that the air jet is surrounded by an annular fuel jet. The second burner (Circumferentially Arranged Ports, CAPs) is an advanced version of CoA burner, where the annular port for fuel is changed into a number of fuel ports. In comparison to the 1st burner, the thickness of the inner tube on the 2nd burner is increased largely to allow a separation between the ejected inner air and outer fuel jets. This separation between fuel and air jets physically intensifies fuel/air mixing. The 3rd basic form of IDF burners is called swirl burner, which utilizes swirling flow to achieve further higher level of fuel/air mixing.

Other forms of IDF burners can be considered as modified versions of three basic burners, with only minute change to the level of fuel/air mixing. For example, triple-tube burner originates from a double-tube burner upon addition of one more tube which provides a shield flow to screen out ambient air from the IDF [58–60]. For another example, increasing the number of fuel ports in CAPs burner arrives at a perforated-plate IDF burner [22]. As a further modification, the shape or size of the fuel ports can be different [61]. Several sketches for these modified configurations of IDF burners are shown in Fig. 1d~f, including triple-concentric-tube burner [17,18,20,35–40,44,58–60], perforated-plate burner [22], burner with varied port shape other than round [61] and back-step burner [27,62].

2.2. Evolution of IDF burners: Trend from diffusion to partial mixing

2.2.1. Laminar & turbulent CoA flame

Most flames practically used are diffusion flames owing to safety reasons. Therefore, higher level of partial premixing is generally desired in diffusion flames to make the flames cleaner. Overall, the evolution from 1st to 3rd burner demonstrates how fuel/air mixing outside of the body of the burner can be intensified to allow more premixed flame features. In early 1984, Wu and Essenhigh [63] fabricated a coflow/coaxial (CoA) burner from two concentric stainless-steel tubes with air supplied through the center and fuel through the annulus. Lab-scale comparison of the normal and inverse mixing configurations was conducted with Re_{air} and Re_{fuel} below 1000. The inverse mixing burner

Table 1
Summary of typical IDF burners IDF categories in previous studies.

Ref.	Year	Burner Conditions	Category of IDF	Focus of Research
Hunger et al. [16]	2017	To co-flows of 95.5 mms and 211.56 mm diameter, surrounding a 5 mm inner diameter nozzle of 0.5 mm wall thickness.	CoA IDF	IDF and NDF are compared in terms of fuel/air mixing field and local flame structure in the turbulent regime.
Zhu et al. [19]	2018	Two concentric stainless-steel tubes. The central tube is 10 mm in diameter and 0.3 mm thick. The outer tube is 40 mm in diameter and 15 mm thick.	CoA IDF	The near-field flow dynamics of laminar IDF, in either reactive or nonreactive case is studied.
Mikofski et al. [20]	2006	Three concentric tubes. The diameters of central annulus and outer tubes are 1, 3 and 6.4 cm.	CoA IDF	Flame heights of laminar IDFs are measured.
Miao et al. [21]	2014	A central hole and twelve circumferential holes with center-to-center distance of 12 mm. The diameters of central and circumferential holes are 5.5 and 2 mm, respectively.	CAPs IDF	Effect of hydrogen addition to liquefied petroleum gas on the lean burning stability of laminar and turbulent IDFs.
Choy et al. [34]	2012	A central hole of 5, 6 or 8.4 mm diameter and twelve circumferential holes of 2.4 diameter, with center-to-center distance of 8, 11.5 or 15 mm.	CAPs IDF	Emission of pollutant and noise from open and impinging IDFs produced by five burners of different sizes.
Zhen et al. [51]	2011	A 6-mm-diameter central air port and twelve circumferential 2.4-mm-diameter fuel ports, with center-to-center distance of 11.5 mm.	CAPs IDF	The nozzle length is found to influence development of flows and interaction between fuel/air jets as well as the pollutant and noise emissions of IDFs.
Zhen et al. [30]	2010	A 12-mm-diameter central air port and twelve circumferential 2.4-mm-diameter fuel ports. Each fuel port is aligned 45° to air port.	Swirl IDF	Flow structure, flame shape, flame length, flame stability and pollutant emission of swirling and non-swirling IDFs are investigated and compared.
Kotb et al. [32]	2016	An air port (13 mm diameter) and 12 circumferential fuel ports (2 mm diameter). Fuel ports are vertically inclined 30° to be in the same or opposite direction of air swirl.	Swirl IDF	The momentum exchange between fuel/air jets of swirl IDF on the flame shape, length and stability are studied. *Co*-swirl IDF is shorter and more stable than counter-swirl IDF.
Patel et al. [53]	2019	Two concentric tubes. The diameters of inner and outer tubes are 19 and 37 mm, respectively. A swirler is installed inside inner tube.	Swirl IDF	The flame length, axial and radial temperature variation and noise level are investigated upon hydrogen enrichment in swirling and non-swirling IDFs.
Paladpokkrong et al. [17]	2018	Three concentric tubes with the diameters of inner, intermediate and outer tubes are 3.86, 15.30 and 32.36 mm, respectively	Tripe tube IDF	The nanostructure and reactivity of soot particles in IDF and NDF
Jung et al. [37]	2012	Three coaxial nozzles. The diameters of inner, intermediate and outer 7.5, 20 and 30 mm, respectively.	Tripe tube IDF	Incipient soot particles are diagnosed to examine the effect of oxygen enrichment on soot zone structure and degree of carbonization in IDFs.
Velásquez et al. [38]	2013	Three concentric stainless-steel tubes. The diameters of inner, intermediate and outer 11, 38 and 75 mm, respectively.	Tripe tube IDF	The chemistry and morphology of soot particles and precursors in IDFs are investigated.
Kapusta et al. [22]	2020	Two coaxial tubes. The diameters of inner and outer tube are 1.6 (or 2 mm) and 30 mm, respectively. A perforated plate is installed at the exit of annulus.	Perforated plate IDF	Different parameters for mapping IDF structures are compared, and the results show that the centre Reynolds number and global equivalence ratio are more universal than jet velocity.
Huang et al. [61]	2005	The central, rectangular slot is 12 mm wide by 95 mm long. Coflow is introduced on each of the long sides of the slot.	Slot IDF	Flame imaging measurements are performed in sooty slot IDFs to diagnose structural features and soot concentrations.
Mahesh et al. [27]	2008	Two coaxial tubes with diameter ratio of 1.8. Inner tube is submerged by 4 mm below outer tube for better fuel/air premixing.	Back-step IDF	The stability and emission characteristics of backstep IDFs are studied and reported.

(*continued on next page*)

Table 1 (*continued*)

Ref.	Year	Burner Conditions	Category of IDF	Focus of Research
Mahesh et al. [62]	2010	The same as [27].	Back-step IDF	The visible flame length, dual flame structure, centerline temperature distribution and oxygen concentration are examined in a turbulent backstep IDF.

produces a bell-shaped blue reaction zone stabilized on the air jet, similar to a normal diffusion flame. The sketch of the burner and flame is shown in Fig. 2a. For such CoA flame in laminar regime, air jet is confined inside fuel jet, which is referred to the phase of prepenetration as discussed later. No bulk convection of fuel into air or vice versa occurs since the thickness of the inner tube is as small as $\delta = 0.7$ mm, and diffusion is the main transport mechanism for fuel/air mixing. Regarding nozzle geometry, it is clear that CoA burner has the simplest configuration among all burners in Fig. 1, but the thin-walled inner tube does not contribute to rapid fuel/air mixing. In the literature, quite many studies rely on the burners of CoA type. To guarantee full confinement of air by fuel and outer tubes with diameter of one or two orders of magnitude larger than inner tubes are generally used [8,12,15,16,19,23,25,41,42,45].

Sze et al. [11] tested CoA flames in a broader flowrate regime, and observed that with sufficient air supplied, air jet penetrates the confinement of fuel. With such high difference in fuel/air velocity, air jet creates a local pressure zone at its root which deflects the outer fuel. The deflection of fuel towards air associates the flow structure with a neck and an overall dual-structure, as illustrated in Fig. 3. In this case, stronger fuel/air mixing over diffusional one occurs due to shear layer formation between coflowing air and fuel jets. Once air jet becomes turbulent, fuel/air mixing is further promoted by turbulence [16,26,28].

2.2.2. *Laminar & turbulent CAPs flame*

Huang et al. [64] a placed a disk at the exit of the inner tube to increase its 'thickness' such that a separation distance of 5.5 mm was established. With low-velocity air jet, four flame patterns were identified according to the central flame features. In all four, the flames could have fuel jet impinging onto air jet due to the enlarged tube thickness. The fuel/air impingement caused by the separation between fuel and air jets incurs bulk and convective mixing between fuel and air. By increasing air jet velocity, the authors observed more flow structures in the phases of transition and penetration in addition to those at the perpetration phase [63]. Three phases of perpetration, transition and penetration are illustrated in Fig. 4. At high air velocity, air jet penetrates the central flame and becomes turbulent, entraining the fuel and leading the flame to expand. While the upstream flame base undergoes an expansion-contraction. Hence, a dual-structure comprising a blue base and a yellow top is formed. Further, this dual-structure IDF is able to turn totally blue under appropriate fuel/air velocity ratio, exhibiting typical characteristic of partially premixed combustion. Sobiesiak and Wenzell [65] mentioned that in laminar regime, diffusion is not the main transport mechanism for this type of flame and the degree of partial premixing depends on fuel entrainment strength that is subject to both nozzle geometry and flow conditions. As far as flow conditions are concerned, Bindar and Irawan [66] suggested air velocity to be 5–16 times higher than fuel velocity to achieve entrainment of fuel into air.

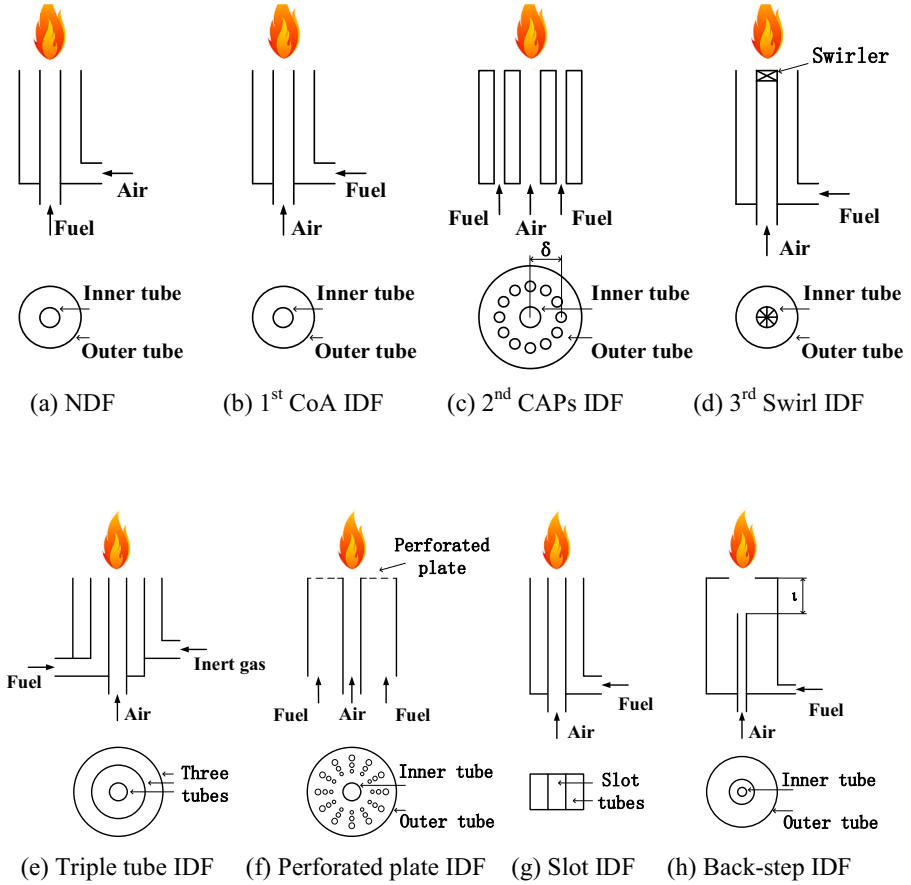

Fig. 1. NDF burner (a) as well as basic (b ~ d) and modified (e ~ h) versions IDF burners.

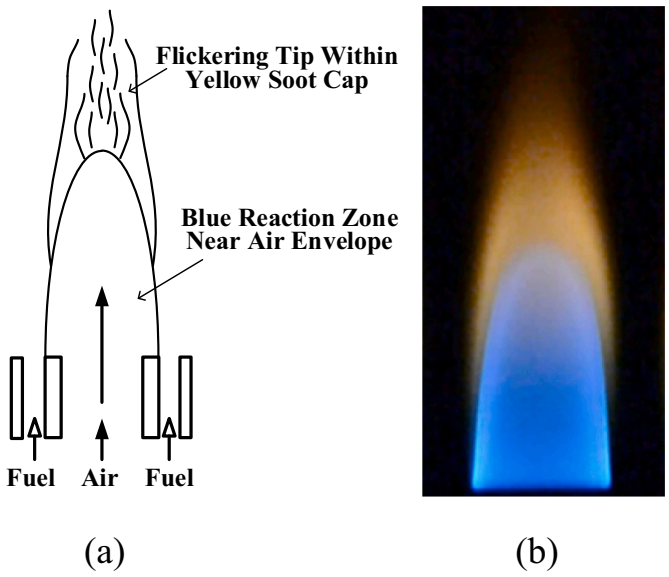

Fig. 2. Laminar CoA IDF: (a) flame sketch in [63] and (b) flame photo in [19]. (Fig. 2b is reprinted from [19] with permission of the Publisher.)

Thick-walled inner tube was later employed by Sze and his co-worker [46], who further changed single annular port into several circumferentially arranged circular ports (CAPs burner). The design concepts of CAPs and CoA were experimentally compared [11], and Fig. 5a and b show the sketches of both burners and flames for CoA and CAPs respectively. The compared results show that the gap between air and fuel ports, formed by the thickened wall of the tube, produces a low pressure zone. The low pressure sucks fuel jets to impinge onto air jet, creating fuel entrainment which contributes to fuel/air mixing. Thus, the CAPs flame has less diffusional features than the CoA flame under most operational conditions tested, such as less yellow plumes that represent soot emission and more occurrences of totally blue dual-structure flames. Besides, CAPs has great ease in modifying flame shapes, appearances, and flow/flame patterns solely by adjusting fuel/air ratio thanks to fuel entrainment. It also possesses advantages coherent in CoA flames, such as broad operational range and safety without flashback. Starting from this prototypical CAPs burner, many modified versions were built for detailed investigation of flow structures, flame stability as well as thermal and emission characteristics of the flames [21,29,33,47–51,54,56,67].

2.2.3. *Swirl flame*

With excess fuel, the post-combustion zone of CoA or CAPs IDFs is very long and sooty. Generally, such diffusional feature of 'long tail' can be curbed by reducing the time required for fuel/air mixing and thus accelerating the combustion processes. Rotational motion has been accepted to be a good technique for stepping up fuel/air mixing in diffusion flames, where swirl can be achieved by swirl vanes or mechanical rotating devices [53]. Using tangential entry of fluid into a cylindrical chamber, Zhen et al. [30,52] built two swirl burners by introducing swirl into air jet. Non-axially moving air parcels grabs fuel, resulting in fuel/air mixing much stronger than the CoA and CAPs concepts. For one design in Fig. 5c [52], the burner head of CAPs was adopted to maintain fuel entrainment at the flame base. Together with the main reaction zone on top of the base, a dual-structure flame is maintained with both fuel entrainment and swirl motion conducive to fuel/air mixing. Note that similar flow/flame structure can be obtained by attaching swirl vanes at the air exit of a CoA or CAPs burner [53]. In another design in Fig. 5d [30], fuel jets on the burner are directly injected into air flow recirculation zone, and a peach-shaped flame with the sole effect of swirl on fuel/air mixing is born. For both designs, turbulence is reinforced by swirl at high Reynolds number and the flames have more nature of premixed combustion. Concurrently, the flames are shorter, wider and more stable than non-swirl IDFs, namely CAPs IDFs under similar operational conditions. Later studies on swirl IDFs can be found in the literature [30–32,52,53,55,68–70].

3. IDF operations and flow/flame patterns

The combustion characteristics of a non-premixed flame strongly depend on its fuel/air mixing rate for which fluid mechanics of the flame would play an important role. The same holds for an inverse diffusion flame. For an IDF, fuel and oxidizer are separated before entering the reaction zone where they mix and burn. Chemical reactions occur only at molecular level, so mixing between fuel and oxidizer must take place before combustion. As chemical reaction rates are fast, the burning rate

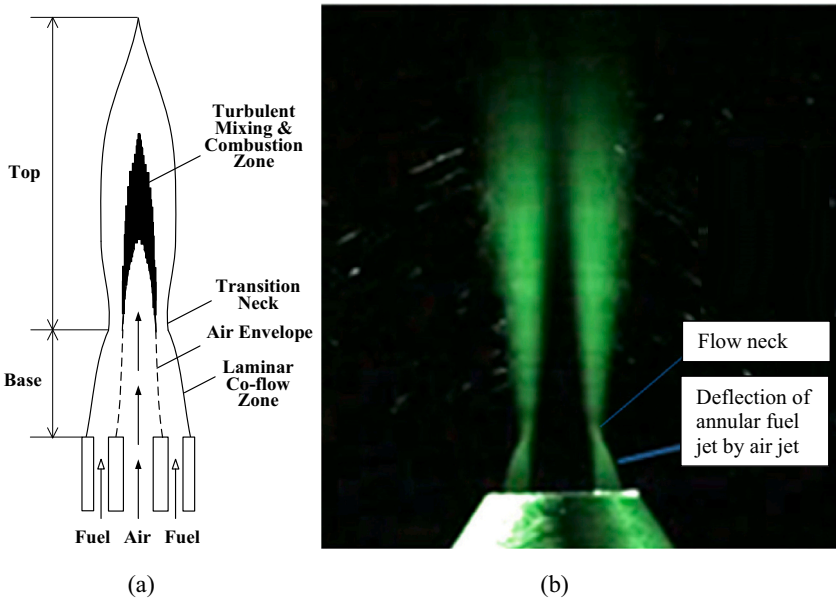

Fig. 3. Turbulent CoA IDF: (a) flame sketch in [11] and (b) flow photo in [26]. (Fig. 3b is reprinted from [26] with permission of the Publisher.)

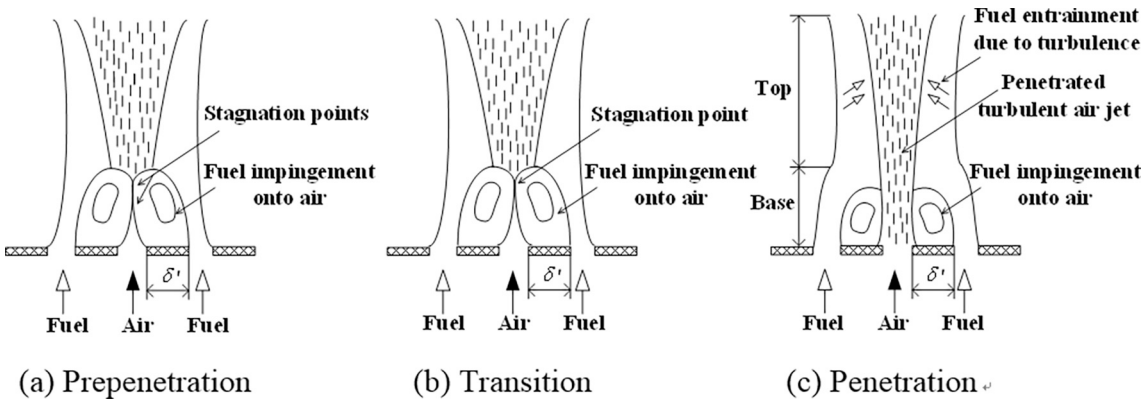

Fig. 4. Sketches of air jet (a) prepenetration, (b) transition, (c) penetration in [64].
(Fig. 4 is redrawn from [64] with permission of the Publisher.)

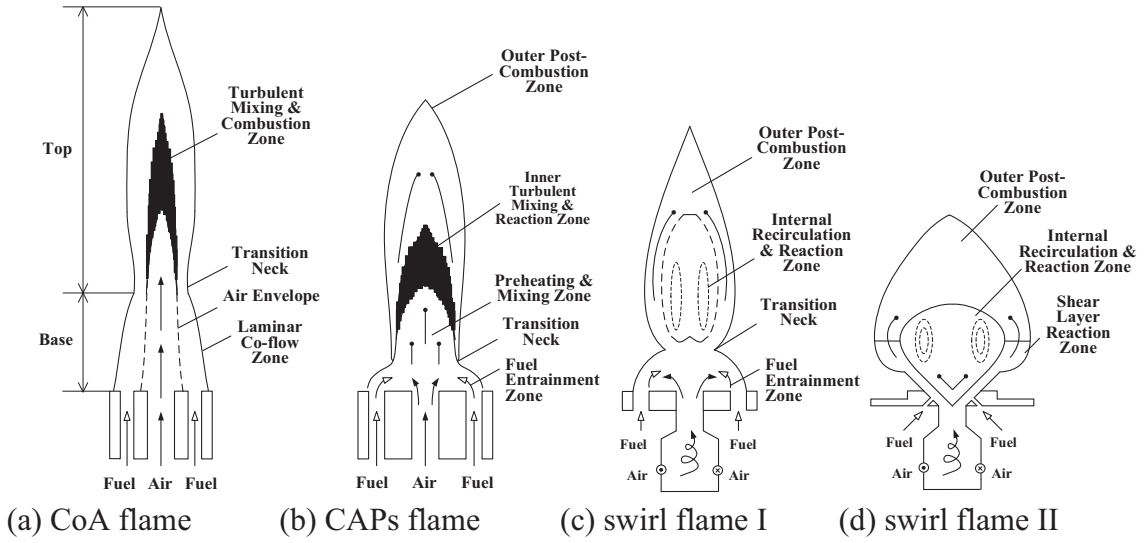

Fig. 5. Sketches of (a) CoA flame, (b) CAPs flame, (c) swirl flame I, (d) swirl flame II.

is limited by the transport process and mixing rate rather than by chemical kinetics. As far as laminar regime of IDFs is concerned, fuel and oxidizer are transported to the reaction zone primarily by diffusion especially for CoA IDFs. While in CAPs or swirl IDFs, more rapid, violent and comprehensive fuel/air mixing can be induced by fuel impingement or radial and tangential flows. Consequently, more combustion features of partial mixing can be gained by CAPs and swirl flames in comparison to CoA flames.

In turbulent regime of IDFs, turbulence steps up the rate and extent of fuel/air mixing, which grants IDFs more features of partial premixed combustion. Previous studies have shown that IDFs can possess excellent turbulent combustion characteristics, such as broad operation range, safety of no flashback, superb flame stability and great ease in adjusting flame appearances (shape/size/length/color) and flow/flame patterns. So in this section, the operation of the basic types of IDFs as well as their flow/flame patterns exhibited in both laminar and turbulent regimes are addressed in details.

3.1. CoA flame

In the study [63], six different flame patterns were identified by varying air jet Reynolds number at $Re_{air} < 1000$ under overall fuel rich conditions. At low fuel velocites, three flames are prone to buoyancy-induced instability. The other three flames (Type I, II and III) formed at high fuel velocities are stable, being representative of the IDFs on the CoA burner. The formation of such three flames with increasing air supply was described by Sobiesiak and Wenzell [65] as: (1) initial introduction of central air causes establishment of an inverse diffusion flame inside the normal flame, both flames attached to the nozzle, i.e. Type I flame in [63], corresponding to perpetration in Fig. 4; (2) a blue reaction zone develops inside the normal flame with a closed tip, i.e. Type II or III flames in [63, 3) further increase in air supply opens the tip, corresponding to transition and penetration in Fig. 4, and finally results in flame blowout.

Upon closer inspection of Type II and III flow/flame patterns, Wang et al. [15] identified two blue zones at either side of the fuel envelope, and compared such double blue zones between IDFs and NDFs. Fig. 6 shows that below the yellow cap of Type II or III IDFs are two blue zones. The inner blue zone is rich in fuel, closed at its tip and thick, while the outer blue zone is stoichiometric, open at the tip and thin. Contrastly, the double blue zones in NDFs are thin and thick respectively at the inner and outer sides, both with closed tips. Moreover, NDFs have lower chemiluminescence than IDFs. The reason is firstly that the fuel- and oxidizer-side emissive species, e.g. C_2* and OH*, are reversed in place between NDFs and IDFs, and secondly the emissive intensities are higher in IDFs due to higher scalar dissipation rates in IDFs.

Before opening of the inner flame tip [63] (transition in Fig. 4), a strong sooting zone is capped by a weak sooting zone, both of which are combined into a flickering (fluctuating) tail of Type-III flame as demonstrated by Fig. 2. With increasing air jet velocities, soot

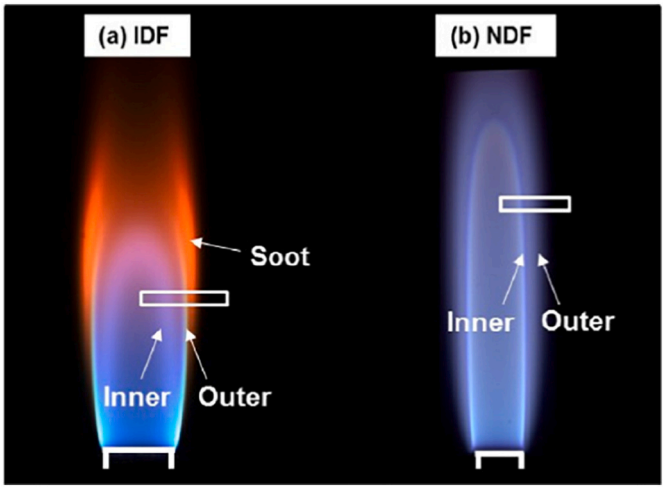

Fig. 6. Double blue zones of Ar-diluted-methane (a) IDF and (b) NDF [15]. (Fig. 6 is reprinted from [15] with permission of the Publisher.)

luminosity and flicker frequency are suppressed [5,26,65,71], and the inner flame eventually blows off the burner as Re_{air} approaches 1000 [63]. Clausing [72] correlated the flame stability data based on a modified Peclet number. Consistency was reported that the Reynolds numbers for inner flame liftoff and blowoff are quite small. This led the authors to claim that laminar IDFs are inherently less stable than laminar NDFs. On the other hand, IDFs have a more stably immobilized stem in the lower portion than NDFs. Zhu et al. [19], by reproducing Type-III flame of Wu and Essenhigh [63] and using a PIV system, revealed that buoyancy-induced vorticity is in the same direction of the vorticity of initial shear flow. As a result, the buoyancy effect depresses the growth of initial shear flow in the near-field, leading to straight and smooth envelope of the flame. While in NDFs, the initial shear flow and buoyancy effect induce opposite-direction vortices, which interact with each other and cause flow instability. The work of Zhu et al. [19] well explained the reason for stabilized stem of Type-III CoA flame. However in the far-field, Kelvin-Helmholtz instability is developed due to further growth of the shear flow, resulting in oscillating flame height and flickering flame tip.

Sobiesiak and Wenzell [65] extended the operation of CoA IDFs from laminar to turbulent regime. With air and fuel velocities respectively up to 50 m/s and 5 m/s tested on ten burners of different air- and fuel-tube diameters, consistent flame dynamics were observed. Starting from laminar CoA flame, increase in air jet velocity initially causes blowout of the inner flame and then a single inverse flame is established. For this single flame, the air jet is normally turbulent while the fuel jet remains laminar. Hence, a laminar diffusion flame is formed near the nozzle and a turbulent flame develops at the upper portion, as illustrated in Fig. 3. The laminar diffusion base is short, consuming a small fraction of fuel. The remainder is abruptly convected around a contracting 'neck' and entrained into the turbulent top overhead. Driven by turbulence of air jet, enhanced fuel/air mixing occurs in the flame top, and a well-premixed reaction zone in the color of blue rides the centerline of the top. The blue reaction zone would be enveloped by an outer diffusion layer given excessive fuel supply. In circumstances depending on the burner and flow conditions, both turbulent top and flame neck turn to blue color. So, together with the blue base, it gives totally blue CoA IDF [26,65]. Generally, blue color is an indicator of premixed combustion for hydrocarbon fuel. Moreover, Sobiesiak and Wenzell [65] recorded steeply rising temperature with axial distance above the burner, and ascertained that such turbulent CoA flames have features of premixed combustion.

Hunger et al. [16] probed the reaction zone of turbulent CoA flame in terms of its species, OH and Rayleigh ratio distributions in mixture fraction space. They disclosed that for highly turbulent CoA flame, the reaction zone experiences shear layer generated turbulence, such that the flamelet structures are embedded in a fully turbulent flow. Therefore, there is no difference in reaction zone flame structures of turbulent IDFs and NDFs, even though it does in laminar regime [20,63,73]. It was found that the flame lengthens with increasing fuel velocity while shortens more dramatically with increasing air velocity [26,65]. When supplied with insufficient fuel, increase in air jet velocity opens the tip of turbulent CoA IDF and eventually leads to flame blowout. At upper flow limit of stability, IDFs extinguish differently as NDFs [65]. Namely, CoA IDFs blow out without prior occurrence of liftoff, and blowout occurs initially to turbulent flame top and then to laminar flame base. Mahesh and Mishra [28] suggested that the short flame base, a unique feature of turbulent CoA IDFs which is formed by entrainment of annular fuel into central air, acts as a pilot flame for the main flame and enhances its stability. Besides, the delayed extinguishment of flame base is ascribed to the reason that its anchoring point is at fuel tube rim and it gets less interference from high velocity air jet [26,28].

3.2. CAPs flame

As clear now, flame base or root is a favorable feature favorable for CoA flame stability and needs to be maintained to new burner design. An updated burner was developed by Sze et al. [46] who increased the 'thickness' of inner tube and replaced single annular port by multiple round ports, as referred to CAPs burner in Fig. 1b. Both update strategies contribute to faster fuel/air mixing at flame root. A sketch of turbulent CoA and CAPs flames is shown in Fig. 5. The major difference between CoA and CAPs is that the fuel in CAPs cannot diffuse into the center of air jet as it does in CoA, but mixes with air midway between the separated fuel and air ports. Hence, flame root is more characterized by an impingement/entrainment zone where the low pressure created by air jet entrains surrounding fuel jets, as illustrated by the sketch in Fig. 5b. Occurring along fuel/air mixing is intense combustion midway between air and fuel ports, incurring high temperature thereunto and heating flame base. Once combustion is initiated at the base, it then propagates upwards. Accordingly, CAPs flame has more intense fuel/air mixing as well as faster combustion than CoA flame under similar operational conditions [11]. This enhanced mixing would arouse earlier transition from partial blue to total blue flame and higher temperature maximal in the flames. In addition, the main reaction zone is closer to the burner and hence the flame can be shorter in the case of CAPs, as indicated by Fig. 5a and b.

Later on, the novel CAPs design and flame features reported in [11,46] provoked many researchers to study CAPs burners and flames [21,29,51,67]. An attempt for a full picture of the flow/flame patterns in wide flowrate regime was made by Dong et al. [29], by increasing air jet Reynolds number (Re_{air}) from zero till flame blowout and overall equivalence ratio (Φ_o) from zero till very rich yellow plume. A total of seven different flame patterns were observed and divided into buoyancy-controlled flames at $Re_{air} < 300$ and momentum-controlled flames at $Re_{air} > 300$. For two buoyancy-controlled flames below $Re_{air} = 300$, there are diffusion features common to laminar CoA flames. While beyond that, five types of flame are formed according to the relative strengths of fuel/air supplies. A totally blue flame is established at $Re_{air} > 4000$, giving a representative dual-structure triple-layer CAPs IDF. Here, dual-structure refers to lower flame base and upper flame torch, and triple-layer includes lower flame base, inner reaction zone and outer diffusion layer of upper torch, respectively. And further, the flame blowout behavior at $Re_{air} = 8800$ resembles that of turbulent CoA flame, i.e. upper flame blows out firstly followed by a delayed blowout of flame base. The wide range of $Re_{air} = 0–8000$ also indicates rather good stability of CAPs flames. Miao et al. [21] tested the lean stablility of a CAPs flame burning liquefied petroleum gas (LPG) or hydrogen-LPG blends. Both LPG-IDF and LPG-H_2-IDF showed superb capability of fuel lean combustion in the range of $Re_{air} = 0–6000$. It was found that

after flame torch blowout triggered by reduced fuel supply, flame base associates with local extinction firstly untill complete extinction occurs. Generally, lean blowout limits of flame torch have a reciprocal relationship with air jet Reynolds number, as it is sensitively subject to shear lifting force and momentum-controlled fuel/air mixing created by air jet. However, as laminar flame base can sustain much high air jet Reynolds number of $Re_{air} > 3000$, and combustion at the base is dominated by fuel/air mixing due to entrainment of fuel into air, Re_{air} less affects flame base blowout limits. Therefore, the special structure of CAPs IDF endows its capability of lean combustion better than NDF or DF. Note that more efforts to improve CAPs burner design can be found in [51,67]. Mainly, geometric quantities of fuel/air ports spacing, air port diameter and port length have been investigated to optimize the combustion features of IDFs. To put it briefly, under identical supplies of fuel and air, smaller air port diameter flame exerts higher flame temperature maximal and wider range of stable operation in terms of both Re_{air} and Φ_o [67]. And shorter air port length flame displays shorter flame base, smaller potential core and thus more compact and intense combustion due to higher turbulence [51].

3.3. Swirl flame

Although CAPs IDF has many advantages such as wider stable operation, lower NO_x emission and less soot luminosity than CoA IDF as reported in the literature [11,46], the flame torch is slimly long. For example, the aspect ratio of dual-structure triple-layer total blue CAPs flame can exceed ten, which was deemed as an inferior feature by Zhen et al. [30,52]. Thus, swirl IDF was developed to reduce flame length and size to achieve more compact combustion. Among three methods of swirl generation, i.e. tangential entry of fluid, guide vanes and rotation of mechanical devices, the authors [30,52] utilized two tangential entries of air in a cylindrical chamber due to its simplicity. Note that the swirl vanes were also adopted by researchers to make swirl IDFs burner [32,53]. As shown in Fig. 5c, the cylindrical chamber acting as swirl generator is attached below the prototype CAPs burner head used in [46], and the resultant swirl flame has a similar dual-structure because of coaxially arranged fuel jets and separated fuel/air ports. In the lower portion, fuel jets are entrained into air jet forming flame base. In the upper portion, recirculating flow induced by swirl develops into main reaction zone inside flame torch. Due to coexistent effects of fuel entrainment and swirl, dual-structure is preserved with triple-layer of flame base, internal flow recirculation/reaction zone and outer post-combustion layer. Direct comparison of this swirling flame with non-swirling CAPs flame showed that the swirling IDF has shorter flame length, more blue coloration and thus more features of premixed combustion [52,53]. All of these can be attributed to the effect of swirl which causes stronger fuel/air mixing and higher turbulence in upper flame torch. However, this swirl burner with coaxially arranged fuel/air ports as well as separated fuel/air ports restricts the development of flow recirculation zone towards larger size and higher strength, such that flame length was observed to increase with increasing air supply [52]. Also based upon the concept of coaxially arranged fuel/air ports, Kotb and Aaad [32] designed a double-swirl IDF burner with both swirling fuel and air jets Helical channels of swirl vanes were used as fuel and air ports, and depending on swirling direction of fuel/air jets, both co-swirl and counter-swirl IDFs were produced and tested. It showed that both flames have an overall dual-structure, i.e. flame base formed by entrainment of fuel into air and flame torch enclosing turbulent reaction zone. No flow recirculation was observed in two flames due to weak swirl induced by the burner. The degree of swirl can be further weakened in the case of counter-swirl, so the co-swirl IDF is superior with shorter flame length, better stability and higher temperature.

Clearly, coaxially arranged fuel/air jets and weak swirl are two factors hindering larger bulk and faster rate of fuel/air mixing. Zhen et al. [30] improved the swirl burner design by enlarging air port, tilting fuel ports inwards and settling both fuel/air ports within a divergent outlet. The result is that fuel entrainment is banned and thus flame base is removed. A short, fat and peach-shaped flame was created, without no cool potential core near the nozzle. In all experimental cases, swirl strength is high and proportional to air supply, with an internal recirculation zone (IRZ) created which grows in size and strength with increasing Re_{air}. Hence, flame length monotonically decreases versus Re_{air}, opposite to the trend in [52]. Different to impingement of fuel/air jets for CAPs flames [21,29,51,67] and weak-swirl flames [32,52,53], fuel/air mixing develops solely owing to strongly swirling flow and shear flow respectively inside and around IRZ. Comparison of such high-swirl IDF to non-swirling CAPs IDF revealed that the swirling IDF has much higher rate of fuel/air mixing, earlier appearance of total blue flame, shorter flame length and thus more compact-size combustion. Besides for fuel/air mixing, IRZ also plays an important role for flame stabilization. It was found that such high-swirl flame is always stably anchored on the divergent nozzle with Re_{air} tested up to 10,000, with no occurrence of local extinction or blowout [30].

4. Lab-scale IDF usages

Traditionally, premixed flames are desired for impingement heating due to its fast connective heat transfer and clean combustion. In past decades, IDF received much research attention because it can exhibit both features of premixed and diffusion combustion, similar to a partially premixed/diffusion flame. However, it is diffusional in nature and thus is safe with no danger of flashback. There is great ease in varying the level of fuel/air mixing, flame appearance, and combustion characteristics by merely adjusting fuel/air supplies. Previous studies have shown that turbulent CAPs IDF or swirl IDF can easily turn into totally blue with less or no soot emission. Further, CAPs or swirl IDFs conquer the need of pilot flame to stabilize turbulent combustion as is the case of partially premixed/diffusion flame. Considering the merits of CAPs or swirl IDFs, these non-premixed flames become an ideal alternative to replace premixed flames in impingement heat transfer applications. In comparison to premixed flames, three outstanding advantages of IDF combustion are: 1) safe operation, with no risk of flashback or blowup, 2) wider operation, with Re_{air} (and thus Re_{fuel}) much higher than the upper limit of $Re \approx 2000$ for purely premixed flame, and 3) higher fueling rate, with no need of pilot flame for stabilization in turbulent regime. Driven by these favorable characteristics of IDF, its impingement heat transfer behavior is explored by many researchers for [29,31,46–50]. Prevalently, most of these studies considered a single vertical flame normally impinging to a flat surface, with thermal and emission characteristics of both free (without plate) and impinging (with plate) flames examined and compared sometimes. This section of the paper, by revisiting benchmark burners, reviews impinging flame structure, thermal flow field and impingement heat transfer characteristics of CAPs and swirl IDFs. For the purpose of better energy efficiency and economy, heat transfer efficiency data reported in the publications becomes the focus of the review.

4.1. Impingement heat transfer

4.1.1. CAPs IDF

Sze et al. [46] are the first authors to propose the usage of dual-structure CAPs IDF for impingement heating. The advantages they reported, are easily adjustable flame length and swiftly transitional flame color from yellow to blue when changing Re_{air} or Φ_o, which consequently alters the heating area of target plate. Dong et al. [47] identified four types of impinging flame structure suitable for heat transfer i.e. flames with 1) impingement of flame base that encloses cold potential core of air jet, 2) impingement of flame torch that comprises closed inner reaction zone and outer diffusion layer, 3) impingement of flame torch containing open inner reaction zone and no perceptible outer diffusion layer, and 4) impingement of flame torch with only outer diffusion layer. Once upon a choice of impinging flame structure for heat transfer, two

important parameters, i.e. flame temperature and gas velocity, need to be considered. Normally, increasing both of them results in higher burning velocity and thus higher heat transfer since the main heat transfer mechanism for impinging flame jets is forced convection [74]. Fig. 7 shows a representative temperature field of free CAPs IDF jet. As can be seen, combustion initiates midway between air and fuel jets in the entrainment zone and develops upwards into the flame torch where the temperature attains its maximal in the flame centre. Testing of impingement heat transfer among four structures reveals that local heat transfer rate on stagnation point (intersection between flame axis and plate surface) becomes maximum when the tip of closed reaction zone impinges the plate. Accordingly, the total heat transfer rate also tends to the highest for this impinging structure with closed inner reaction zone. In order to achieve this structure and thus highest heat flux, overall equivalence ratio should exceed one, so that a fuel-rich mixture allows a diffusion layer to close main reaction zone. Additionally, nozzle-to-plate distance (H) should match the height of reaction zone tip. If overall equivalence ratio or nozzle-to-plate distance becomes too high or too low, stagnation point heat flux drops, which indicates an existence of optimum Φ_o and H. That means for each Re_{air}, there exists an optimum Φ_o coupled with an optimum H to achieve highest stagnation point heat flux and total heat transfer rate. As is found [47,67], such optimum Φ_o for IDF is generally larger than that for premixed flame, which is around one or slightly over one. This difference in optimum equivalence ratio for heat transfer originates in relatively poorer air/fuel mixedness in IDF which is diffusional in nature. Moreover, turbulent IDF entrains more ambient air due to its higher turbulence than premixed flame, such that complete consumption of supplied fuel demands overall equivalence ratio to be over one.

The reported data by Ng et al. [48] show that although total heat transfer rate monotonically increases with either Re_{air} or Φ_o at fixed H owing to raised thermal energy input, heat transfer efficiency shows no such monotonic trend. Heat transfer efficiency, defined as total heat transfer rate divided by input thermal energy of impinging flame, is an indicator of how effectively the energy is used. As far as flame impingement heating is concerned, chemical energy of supplied fuel is converted to thermal energy through combustion and is further transferred to impingement target. A figure summarizing the published data in terms of heat transfer efficiency is presented in Fig. 8. In the study

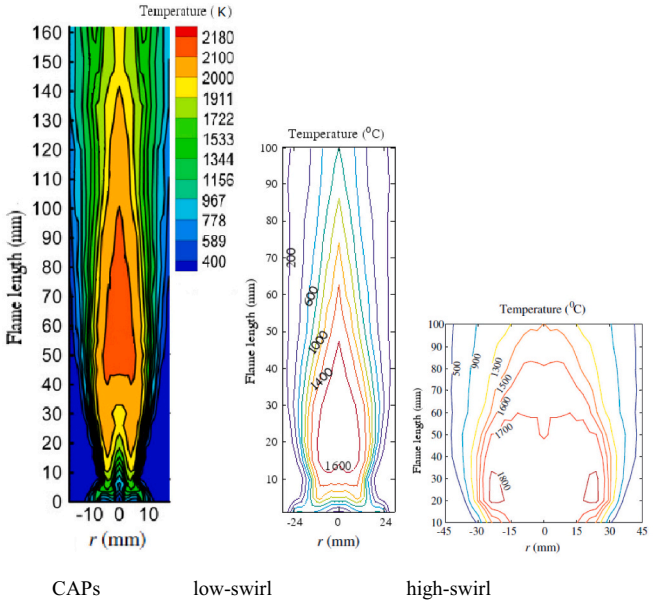

CAPs low-swirl high-swirl

Fig. 7. Thermal temperature fields for free CAPs IDF [67], low-swirl IDF [52] and high-swirl IDF [55].
(Fig. 7a is reprinted from [67] with permission of the Publisher.)

[48], heat transfer efficiency under the operation of $Re_{air} = 2000$ and $H/d_{air} = 5$ attains a maximal at $\Phi_o = 1.2$ and drops on both sides of $\Phi_o = 1.2$. For different air jet Reynolds numbers, the maxima occur at $\Phi_o = 1.0$ and 0.8 for $Re_{air} = 2500$ and 3000, respectively. In another study [49], the flame under $Re_{air} = 4000$ and $\Phi_o = 1.4$ shows a highest heating efficiency at $H = 7.5d_{air}$ which is also the optimum nozzle-to-plate distance for maximum total heat transfer rate. Under fixed $\Phi_o = 1.4$ while increasing Re_{air} from 3000 to 6500, the efficiencies obtained at their own optimum H shows a monotonic decrease. When identical fuel and air flow rates are supplied among three burners with different air port diameters, smaller air port flame associates with higher heat transfer efficiency. From the studies, it is seen that any of the parameters of Re_{air}, Φ_o and H as well as burner geometry affects heat transfer efficiency. Therefore, in heating applications, users may firstly estimate thermal power required, specify Re_{air} or air supply required and then adjust fuel supply and nozzle-to-plate distance to achieve highest energy efficiency and best economy as well.

Intuitively, one would quickly spot the highest heat transfer efficiency in Fig. 8 to be 79% in the study [48], and regard this CAPs IDF's corresponding burner geometry and operation as the best. However, all data in the figure are within some restrictions set in each literature, and thus they are of reference value only. The restrictions can be any two parameters from Re_{air}, Φ_o and H to be constant or fuel/air flow rates to be fixed. Note that for each pair of Re_{air} and Φ_o, heat transfer efficiency has an optimum nozzle-to-plate distance to achieve a maximal. Clearly, not all efficiencies in Fig. 8 correspond to their optimum H when Re_{air} and Φ_o are fixed, and in some literature only scarce pairs of Re_{air} and Φ_o are examined. That is to say, more complete information on energy usage efficiency of IDFs is still in lack, and improvement can take this way. For each burner design, a wide range of operation need to be tested to recognize its highest heat transfer efficiency. Towards this destination, some data missed in the literature are to be replenished. Afterwards, more reasonable and precise comparison of these efficiency maxima is possible to identify highest energy efficiency achievable by CAPs IDF and corresponding burner geometry and operation. To conclude, as far as current published data are concerned, the highest heating efficiency is 79% for the IDF under $Re_{air} = 2000$ and $\Phi_o = 1.2$ [48]. However, the picture of heating efficiency in Fig. 8 is incomplete as many previous works does not focus on identification of highest heating efficiency. More work needs to be conducted in the future, in order to find which design and operation are the best in terms of efficient energy use.

Another facet of reported efficiency data indicates that CAPs IDF can possess comparable or even higher heat transfer efficiency than premixed flame. Ng et al. [48] precisely compared the efficiency maxima between CAPs IDFs and premixed flames under identical flow rates of both fuel and air. Fig. 8 shows that the efficiency maximal of CAPs IDF is higher than that of premixed flame. Dong et al. [47] compared the heat transfer rates of CAPs IDF and premixed flame. The latter operates under $Re = 2500$ configured with optimized parameters of both equivalence ratio and nozzle-to-plate distance, while the former burns under $Re_{air} = 2500$, $\Phi_o = 1.0$ with the same normalized nozzle-to-plate distance of 5 as premixed flame. So, the premixed flame is yielding the highest heat transfer efficiency while the IDF is not. Even though, the heating efficiency of IDF is higher than premixed flame. It is expected that by further configuring IDF under optimum operation, IDF is a better energy-efficient technique to convert and deliver thermal energy from flame to impingement target.

4.1.2. Swirl IDF

With an effort to make IDF a successful and better alternative of premixed flame in practical heating applications, shorter and more compact flame is realized by the use of swirl. The first rigorous research on swirl IDF with swirling air jet was carried out by Zhen et al. [52,68]. In their comparative study of swirling and non-swirling CAPs IDFs, both with coaxially arranged fuel jets [52], the effect of low-swirl was

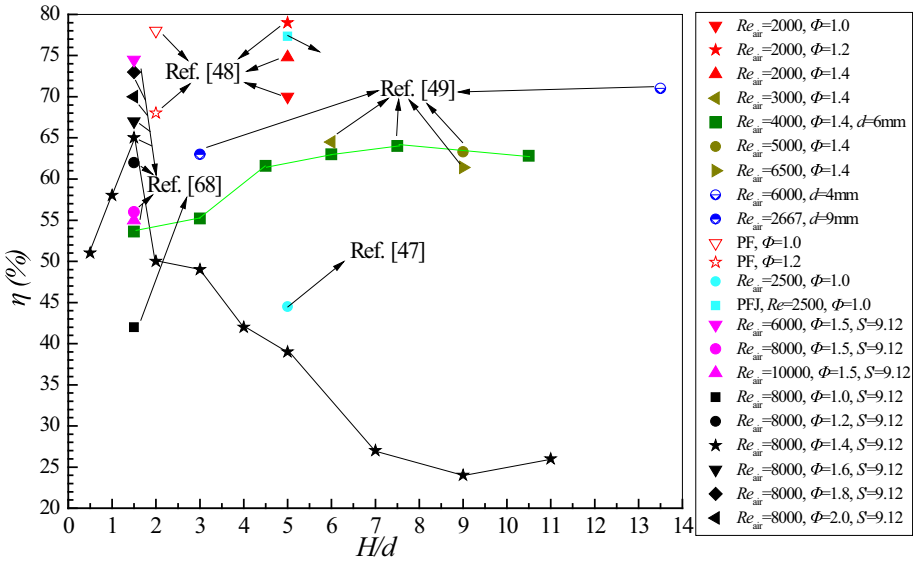

Fig. 8. Heat transfer efficiencies reported in the literature [47–49,68].

researched with several differences in flow field clarified: 1) presence of swirl destroys potential/cool core at flame base and moves high-temperature reaction zone closer to burner, 2) at flame base, swirling CAPs IDF has no negative wall static pressure while non-swirling CAPs IDF does, 3) profile of wall static pressure at flame torch is M-shaped while bell-shaped for swirling and non-swirling flames, and low-swirl IDF has no reverse flow, 4) main reaction zone is wider in swirl flame with lower wall static pressure due to angular gas velocities, and 5) once upon impingement, swirl flame has larger contact area and lower wall static pressure. Therefore, according to the heat transfer mechanism of forced convection with dominant influencing factors of gas temperature and velocity, it is straightforward that lower wall static pressure of swirl IDF results in lower heat flux, leading to M-shaped heat flux profile, while that of non-swirl IDF is bell-shaped. Much stronger swirl strength was used in the study [68], which changed fuel jets from coaxially arranged to tilted towards air jet. The effect of high-swirl was found to be: 1) disappearance of cool potential core of air jet near burner exit, 2) shorter and fatter flame in comparison to low-swirl flame, 3) M-shaped profile of wall static pressure with negative value, 4) formation of internal flow recirculation zone (IRZ), and 5) a governing role played by IRZ for shorter flame length, more compact combustion and higher flame stability.

A typical thermal field of low-swirl CAPs IDF is presented in Fig. 7. As low-swirl CAPs IDF reserves the configuration of coaxially arranged fuel jets and hence maintains a dual-structure composed of flame base and torch [52], its impinging structure can be classified similarly as a dual-structure non-swirling CAPs IDF [47]. Nevertheless, impingement testing indicates that among all impinging structures, swirl reduces impingement heat transfer. The reason is that angular gas velocity reduces axial velocity normal to target surface, resulting in lower wall static pressure and lower heat flux at stagnation point, even though flame temperature tends to increase by stronger fuel/air mixing due to swirl. So, for higher heat transfer, optimum nozzle-to-plate distance should match the height of lower edge of main reaction zone to avoid severe decay of axial velocity. Fig. 7 also gives a representative temperature field of high-swirl IDF. IRZ resides in the center of peach-shaped flame with relatively high and uniform temperature distribution due to well-stirred flow condition thereunto. Enclosing IRZ are premixed and diffusion layers in lower and upper sections respectively, and thus three-zone structure is formed. Accordingly, there are three types of impinging structure, i.e. flames with impingement of IRZ and outer premixed layer, impingement of IRZ and outer diffusion layer and impingement of diffusion layer tip, respectively. As reported, IRZ is a favorable factor for cutting flame length, boosting fuel/air mixing and enhancing flame stability. But it has adverse effect on heat transfer, as reverse flow deteriorates impinging gas velocity. As for heat transfer efficiency, the effects of Re_{air}, Φ_o and H are shown in Fig. 7. There are several operations of high-swirl IDF with over 70% efficiencies, hinting a not too low efficiency for impinging IDF with high-swirl. On the other side of coin, swirl IDF is shorter in length, shorter in optimum nozzle-to-plate distance and thus the system of burner-plate is more compact than low-swirl and non-swirl IDFs. Besides, swirl flames have more uniform heating than non-swirl ones [52,68].

Pollutants emitted from impinging flame are also of great concern, as they directly apply to human nearby. CO, HC and NO_x are major gaseous pollutants considered in the literature. CO is most concerned as it is hazardous and may incur health problems. There are inherent inter-relationships among flow/flame structure, temperature and gaseous species, so typically all quantities are concurrently measured in open and impinging IDFs [11,29,33,46,51,55,67,69]. Importantly, pollutant species formation and growth in different burners are significantly affected by temperature-time profile. For those species that are sensitive to radical species, the radical concentrations in different burners will also affect pollutant formation and decomposition. Further for impinging circumstances, flame-wall interaction also needs to be considered. Generally, impinging flame emits less NO_x and more CO than corresponding open flame [69]. While swirl flame has lower emission index of CO than corresponding non-swirl flame, due to a favorable effect of reinforced fuel/air mixing in curtailing CO emission [69]. A consensus from previous studies suggests less impingement of main reaction zone of either non-swirl or swirl flame for lower CO/HC emissions. Therefore, from an overall viewpoint of heat transfer and pollutant emission, optimized nozzle-to-plate distance need to match the tip of main reaction zone.

4.2. IDF & soot research

In addition to gaseous air pollutants of CO//HC/NO_x, soot particle is another regular but solid-state pollutant emitted by flames. Due to its high environmental and health risks, soot formation mechanism has been studied by many researchers, which is the basis for finding better mitigation strategies to control and reduce soot emission. In fact, IDF employed for laboratory research has been forged into a standard flame for soot inception studies [18,36,37,39]. The IDF technology has proven

advantageous for 'young soot' studies because of its unique flow and combustion characteristics. That is, fuel pyrolysis zone and oxidation zone are separated. Due to same reason, it is suitable for carbon nano-material synthesis [41–45], and the R&D importance of IDF to create new materials of nano-tube, nano-fibers and functional devices have been recognized by many researchers in past decades. What is common is that both soot and carbon nano-material are initially composed by fused aromatic nuclei with their later evolution impacted by burner design, fuel type, flow field and combustion conditions of IDF. As this paper has been focusing on different burner designs, fuel/air mixing and flow field features of IDFs in preceding sections, review of sooting IDFs will continue in this section with emphasis on how species mixing and fuidynamic transport affects flame's sooting characteristics.

Formation of soot is an extremely complex process, which is accompanied by multiple physical interactions and chemical reactions [75–77]. Briefly, it is divided into two phases, gas-phase and particle-phase chemical kinetics, respectively corresponding to soot inception and soot particle nucleation and growth. The prevalently acceptable mechanism of soot formation from fuel molecules to nascent soot particles includes: fuel pyrolysis, nucleation, surface growth, coagulation and agglomeration [78–80]. During all phases of soot formation, particle oxidation occurs all the time due to the presence of O, OH and other oxidizing radicals. It is now popularly accepted that formation of PAHs (Polycyclic Aromatic Hydrocarbon) is the key step in bridging the gap between gaseous fuel molecules and solid soot particles. Universally, the factors influencing PAHs formation involve: fuel and its pyrolyzed species, reaction temperature, pressure and flow field characteristics. The specific reasons are as follow. Firstly, fuel and fuel pyrolysis are important for soot inception. When hydrocarbon pyrolyzes inside a high temperature environment with deficient oxygen, the types of pyrolyzed species, their concentrations and production rates impact PAHs formation as well as their reactions with acetylene (C_2H_2). Secondly, flame temperature plays an important role for soot formation, as the rates of fuel pyrolysis and of PAHs and C_2H_2 production depend crucially on temperature. In addition, soot inception only occurs at temperature approximately over certain temperature, e.g. 1350 K in an axisymmetric laminar diffusion flame [81] and 1000 K in a jet-stirred reactor [82]. Thirdly, pressure incurs changes in chemical reaction rates, thus exerts an effect on soot inception. Lastly, sooting behavior of a flame is greatly influenced by flow field characteristics, because many influencing factors of soot formation and oxidation, such as species concentration, species diffusion, residence time, temperature, particle path and etc. are coupled to fluid dynamics.

4.2.1. Laminar IDF soot

Sooting mechanism in NDF or IDF is difficult to interpret when compared to counterflow flames, because of intrinsically two- or three-dimensional flow structure and more complicated fluid dynamics. To avoid even more complex effect of turbulent fluid dynamics, laminar flames are preferred in most studies, respective of counter-flow flame, IDFs or NDFs. Therefore, a majority of previous studies on IDF soot reply on laminar IDFs, due to its relatively simple and measurable flow field. Generally, coaxial triple-tube IDF burners other than double-tube ones are preferred for soot studies as the outermost inert gas jet acts as a shield to prevent burning of fuel with room air.

To examine the effect of laminar flow-field, Kang et al. [83] carried out an experimental comparison of laminar IDF and NDF. They found that overall soot formation mechanisms are just similar between two types of diffusion flames. However, two flames have a major difference in terms of the relative transport of soot particles to flame, which is schematically illustrated in Fig. 9. In NDF, soot particles are transported towards high temperature flame and experience the processes of soot inception, growth, coagulation and oxidation. While in IDF, soot particles are transported away from flame without experiencing oxidation and finally they leak out of flame. According to the authors, IDFs and NDFs fall into the categories of soot formation flames and soot formation-oxidation flames, respectively [83].

Kaplan and Kailasanath [84] conducted a comprehensive study of both NDFs and IDFs, using a code to predict sooting rates of nucleation, surface growth and oxidation. The laminar IDF, i.e. the CoA flame experimentally tested by Wu and Essenhigh [63], has significantly different sooting behavior from NDF. First, soot formation is much less in IDF. Second, soot forms on the top region of IDF while it occurs within low- to mid-annular regions of NDF. Third, both rates of nucleation and surface growth are lower in IDF, and soot oxidation rate due to OH and O_2 is lower, too. Fourth, soot oxidation in IDF is mainly due to O_2 within mid-region that is right above flame sheet, while in NDF it is due to OH located at the flame top. Fifth, surface growth continues after oxidation has ceased in IDF, causing IDF to emit 'young soot'. By examining soot particle pathlines, the authors ascribed the above distinct sooting characteristics of IDF to its inverse fuel/air jet configuration, and resultant particular flow field or combustion condition as well. These include: 1) axial velocity at low flame height peaks on flame centerline of IDFs while peaks in annular region of NDFs because temperature of annular region is greater than central region. 2) IDF in laminar regime is under-ventilated with O_2 in reaction zone completely depleted, and thus reaction zone is closer to burner compared to NDF. As a result, these differences, soot particles in IDF start to form in a fuel-lean region near burner. Then they pass through stoichiometric reaction surface and travel with increasing mixture fraction while decreasing temperature. Typically, soot nucleation begins after the particles have crossed flame sheet and thus the sooting zone is above stoichiometric reaction surface. In contrast, soot particles in NDF form in a fuel-rich region and travel with decreasing mixture fraction and increasing temperature towards stoichiometric surface.

Driven by distinct flow fields, soot particles in IDFs and NDFs have different histories of temperature, stoichiometry and residence time. In nature, IDF is less luminous and less sooting, and soot existent in IDFs are younger due to lesser oxidation of the soot formed. Blevins et al. [58] referred to these particles which are large and partially carbonized as "young soot", since soot in IDFs is expected to cool and quench immediately after formation. The authors further found that young soot is chemically similar to precursor soot and morphologically similar to soot in underventilated flames. Investigation of young soot containing PAHs is very important as it can reveal initial stages of soot formation as well as transition from early precursor particles to carbonaceous soot. Compared to NDF, sampling of larger quantities of precursors is facilitated by flow field of IDF due to the following reasons. Soot formation in IDF is on fuel side and is convected axially along outer edge of flame until it exits without passing through oxidizing flame tip. In contrast, soot in NDF forms at flame center and experiences appropriate time/temperature/species conditions leading to carbonization and oxidation when approaching flame tip.

Residence time is an important factor related to the flow-field characteristics that influence surface growth rate of soot and thus affect soot formation. Strain rate is another important flow-field-derived factor affecting soot formation, as counterflow flame studies have shown that sooting counterflow flame becomes soot-free at high strain rate. Additionally, fuel/air mixing is also a flow-field factor that change soot formation, given that the chemistry of soot inception demands high temperature and fuel/air mixing vary local gas composition and temperature. All these factors can be easily varied by changing fuel-to-air velocity ratio on an IDF. Lee et al. [85] tested various laminar CoA IDFs and obtained a stability map similar to that of Wu and Essenhigh [16]. For Type III flame, an increase in fuel velocity results in lower C/H ratio and reduces residence time which will delay soot carbonization, while an increased air velocity induces longer flame, higher C/H ratio and more carbonized soot due to longer residence time by high temperature flow field. Katta et al. [35] concentrated their attention to the interaction of vortices with species and temperature for a flickering Type III flame on a triple-tube IDF burner. Through detailed-chemistry flow-field simulation, buoyancy-induced vortices are observed to establish

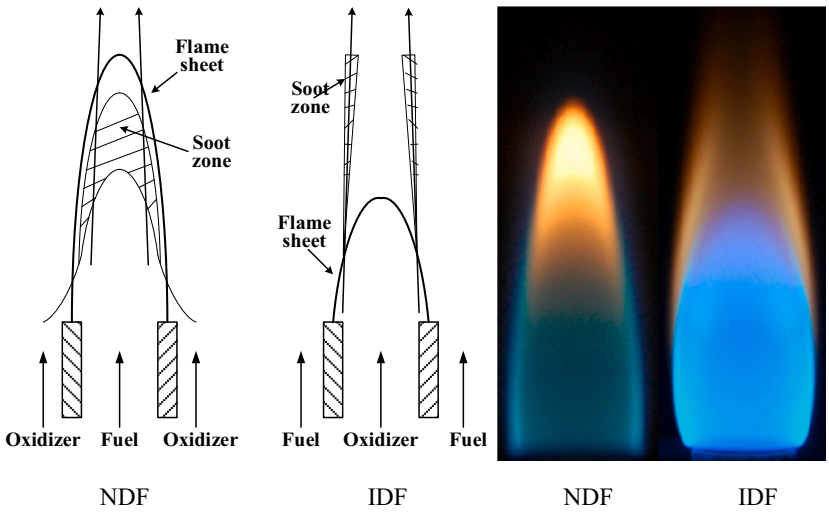

Fig. 9. Schematic different flow fields (left, [83]) and flame photos (right, [89]) of NDF and IDF.
(Fig. 9 is reprinted from [89] with permission of the Publisher.)

outside flame surface on fuel side and advect into exhaust gas. While in NDF which has less stable flame stem in lower flame portion, vortices primarily appear within flame surface [19]. As a result of better stabilized flame stem of IDF than NDF, transport of PAHs species and soot particles closely follow the streamlines of flow in the flame stem region. Near flickering flame tip, the advection of buoyancy-induced vortices promotes mixing between combustion products and cold fuel. Simultaneously, PAHs species and soot particles are entrained into these vortices to increase their residence times. Soot particles could be cyclically heated and cooled while being entrained into and advected by these vortices near flame tip, leading them more susceptible to surface growth, coagulation and carbonization. Apart from the changes caused by varying fuel-to-air velocity ratio to residence time, fuel/air mixing and local flame structure/temperature, strain rate is also changed. Borrowing the findings from counterflow flame of Wang and Chung [83], progressively higher strain rate (shorter residence time) sequentially leads to disappearance of soot, PAHs and eventually flame extinction. Although strain rate in laminar IDF is so low and thus has not been observed to incur soot or PAHs disappearance, an overall similar trend will stand for IDF once extended into turbulent regime.

Laminar IDFs open the possibility of extensive research on young soot, i.e. early soot at inception stage before surface growth. In IDFs, soot and intermediate products do not pass through main reaction zone and thus avoid significant oxidation and carbonization. Such particular configuration of IDFs allows large samples of incipient soot to be annularly gathered without need to invade flame center by using sampling probe. Once sampled, various measurements such as transmission electron microscopy (TEM) images, C/H ratio, LMMS and GC/MS can be performed to explore the soot characteristics. By transiently inserting a TEM grid along the sooting line of laminar IDF where soot concentration

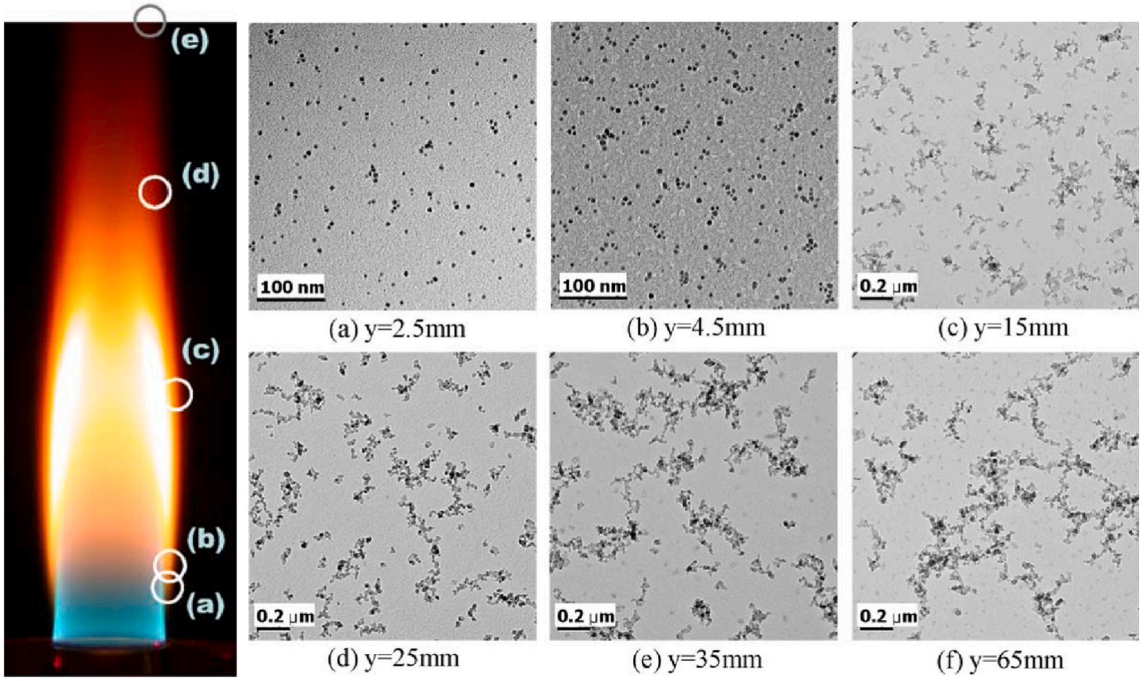

Fig. 10. TEM photographs of incipient particle and aggregates captured on a carbon grid along the soot maximum line in an ethene IDF [87].
(Fig. 10 is reprinted from [87] with permission of the Publisher.)

is maximum, Oh et al. [84] obtained young soot at different flame heights. As illustrated in Fig. 10, TEM provided visual pictures of the soot morphologies. Katta et al. [35] found that IDF does not expand in radial direction downstream of burner exit, because the equivalence ratio sustaining lean combustion is so low that there is deficient fuel diffusing into oxidizer and establishes flame surface on air side. In the region near nozzle exit (positions a-b in Fig. 10), coagulated PAHs are seen as a semitransparent tarlike material, and precursor soot exhibit regular crystalline-layered structure covered by tarlike material. These young soot is sticky, vicious and enriched with hydrogen. With progress to higher flame positions (positions c-f in Fig. 10), young soot as well as their aggregates undergo surface growth and coagulation/coalescent collision growth. In these processes, they are transformed into carbonaceous soot where high temperature results in dehydrogenation and formation of a partially graphitic structure. From Fig. 10, it is not difficult to see that laminar IDF has rather simple flow fields and well defined sooting lines. In this case, soot particles just follow straight or curved flow streamlines [85], thanks for stabilized flame stem and diffusional fuel/air mixing flow field which is lack of turbulence complexity. Furthermore, axial velocity of buoyancy-controlled laminar flames has a constant acceleration regardless of the locations of streamlines. To conclude briefly, laminar IDFs render great ease for tracking chemical and physical pathlines of soot particles. Therefore, extensive studies have been carried out on laminar IDFs to investigate the effects of residence time, temperature, fuel dilution, oxygen enrichment, H_2 addition and CO_2 addition on incipient soot formation, growth and oxidation processes [37,39,81,84,86–88]. Also, a redundant branch of studies have been conducted on the morphology, nanostructure and oxidation behaviors of young soot formed in IDFs [17,18,40,89–92].

4.2.2. Turbulent IDF soot

In practical combustion devices, turbulent flames are definitely more prevalent than laminar flames. Thus, laboratory investigation of flow/flame characteristics directly using turbulent flames is of greater significance. However, as far as the sooting behaviors of inverse diffusion flames are concerned, scarce studies have been made in turbulent regime. It may be due to the following reasons. First, turbulent IDFs have more complex factors influencing soot formation and decomposition than laminar IDFs, and many of these factors are turbulence/combustion coupled. Second, the method of particle tracking adopted in laminar IDFs to examine time/temperature/PAH-chemistry pathways of incipient soot particles is very costly to perform in turbulent IDFs, due to their time-varying chemical and temperature environments. For such diagnostics, both spatially and temporally-resolved measurements of temperature, species and turbulence are required. Third, an attractive and popular technique for sooting turbulent flame studies is numerical simulation. During development of numerical models for sooting turbulent flames, soot reaction mechanisms are firstly developed, tested and refined in laminar flame and then are used as inputs to turbulent flame models. However, solely modelling of turbulent flow itself has many unanswered questions. Therefore, a proper simulation of soot reactions in turbulent flames depends on reliable modelling of turbulence, chemical kinetics and their mutual interaction, together with a good knowledge of the impacts of influencing factors such as local stoichiometry, species concentration, temperature, velocity, turbulence, vorticity, strain rate and etc. Clearly, due to scarcely available experimental and numerical data in the field of sooting turbulent IDFs, our current understanding about soot formation and evolution in turbulent flames is far from complete. In this section of the paper, an attempt to review current data on turbulent IDF soot is made. However, very scarce data are found in this field, so it is unclear whether there are particular sooting features of turbulent IDFs in comparison to other diffusion flames. Instead, in order to update the researchers working in the field and propel the research work forward, this section introduces some influencing factors arising from turbulent IDFs as well as DFs that need be considered in future studies of soot formation and evolution in turbulent IDFs.

Distinct to laminar flames, turbulence plays a role in soot formation and oxidation in turbulent flames. Evidence has been given by Magnussen et al. [96] that an increase in Reynolds number incurs a significant reduction on the amount of soot formed. In their study, on-site laser diagnostics of soot concentration was realized by light scattering technique. Due to turbulence, soot concentration fluctuates in upper/later stages of the flame, and maximum soot concentration locates at nearly the same axial distance from burner nozzle regardless of Re_{air}. Both results reveal a different sooting feature between laminar and turbulent flames. One the one hand, the soot formed in later flame stages is more homogeneously distributed in turbulent flames. The authors [96] reported that higher turbulence reduces more soot by finding lower soot concentration at higher Re_{air} and soot inception delayed to higher axial distance. They attributed the reason for soot reduction to decreased residence time caused by higher turbulence (Reynolds number).

Eddy is a flow phenomenon due to vorticity. A turbulent flow comprises eddies with a multitude of sizes and vorticities. For a free jet diffusion flame, the greater the Reynolds number, the wider the range of eddy sizes from the smallest to largest. The experiments of Magnussen [97] disclosed that towards the edges and tail of turbulent flame where soot is heavily formed, eddy also develops. The effect of turbulence leads to a highly intermittent appearance of soot. This pattern of eddy-initiated soot was further confirmed by numerical data [96,98]. It shows that soot grows in a way similar to turbulence eddy growth and burns away as bigger eddies break up into smaller ones. Therefore, it was believed by the authors that soot is formed and contained in eddies in turbulent flames.

Strain rate has an important effect on soot formation and transport in both laminar and turbulent flames. It has been well known that a sooting counterflow flame reduces levels of soot emission or even becomes soot-free by increasing strain rate [86]. The definition of strain rate is commonly referred to as the axial velocity gradient in fuel/air mixing layer of a flame [99]. Parametric studies on strain rate effects are typically carried out in counterflow flames due to the ease in strain rate quantification. The effect of strain rate is also necessary for investigation in free jet flames. However, strain rate in jet flames is hard to determine and instead qualitative analysis is often sought by researchers. Qualitatively, strain rate is proportional to jet velocity and inversely proportional to residence time or Damköhler number. Strain rate is also closely related to scalar dissipation rate (mixture fraction gradient), a parameter embodying the rate of fuel/air mixing. It seems that upon interaction between soot formation and transport, these physically intercorrelated factors can be similarly interpreted. For example, when jet Reynolds number of a diffusion flame increases, global Damköhler number (a ratio between flow time and reaction time) or residence time (a ratio between flame length and jet velocity) tends to decrease while strain rate would increase. One common effect of three parameters is to reduce global soot emission. Following increased strain rate, fuel/air mixing rate and mixing layer are prone to enhance and enlarge respectively, which in turn alters scalar dissipation rate (mixture fraction gradient). It is generally accepted that soot only forms at low scalar dissipation rate [100], which is in close agreement with the statement that there exists a critical strain rate beyond which soot formation is not possible [100,101]. However, turbulent flow/flame is very complex due to its wide ranges of length/time scales. So, though global parameters aforementioned can be intuitively correlated, the relationship among local parameters as well as their effects on soot formation/evolution is far more intricate and incompletely understood yet.

Now, several fluidynamic parameters affecting soot formation in turbulent flames have been introduced briefly. Experimentally, in-situ and simultaneous diagnostics of multiple transport parameters as well as soot volume fraction, number, density and etc. are needed. Numerically, further detailed information about the interaction between flow

field and soot formation/decomposition can be obtained from models validated by experiments. Besides such kind of in-situ analysis, ex-situ studies on physical and chemical characteristics of soot emitted from turbulent flames are also important because such studies provide insights to not only soot formation/evolution processes but also their negative impacts on environment and human health [102]. Compared to the progress achieved on soot formation/evolution in turbulent free jet diffusion flames, our understanding of soot in turbulent IDFs is less advanced. Previous investigations mainly examined the sooting characteristics of IDFs as well as their differences to NDFs in laminar regime. Extending previous studies from laminar to turbulent demands both resolved results of flow field and soot characteristics of turbulent IDFs. Therefore, not only flow field data of turbulent IDFs [16,22,23,25,54,103] are necessary, but also the studies relating these results from IDFs to the corresponding NDFs are needed [16].

5. Concluding marks and further recommendations

Driven by the interest in adoption of inverse diffusion flame (IDF) in practical devices for efficiently retrieving energy from fuel and effectively reducing air pollution, plenty of laboratory burners have been tested for fundamental studies of IDF flow and flame behaviors. In this paper, a thorough review of the laboratory studies of IDF has been presented. Classification of the burners was made, operation of the flows/flames was clarified, and the flow field, thermal field and combustion characteristics of IDF were expounded. Two major applications of IDF were introduced, i.e. turbulent IDF for impingement heat transfer and laminar IDF for fundamental understanding of sooting mechanism. Overall, the review centers on the role of fuel/air mixing on flow and flame behaviors, as fuel/air mixing is a key factor altering the partial premixed combustion features of IDF which is diffusional in nature. Drawn from the review are the following suggestions.

As for turbulent IDF, either non-swirl or swirl flame of CAPs concept has been identified feasible for impingement heating applications. As major challenge for future design of heating burners is aiming at more environmental-friendly, higher heating-efficiency and lower operating and fabrication costs, improvement in burner design and refinement of optimum operation is still necessary. As fuel/air mixing occurs outside of the burner, flames using fuels of relatively high flashback possibility such as H_2 can be explored without risk of flashback. Because IDF is restricted by relative poorer molecular mixedness in comparison to premixed flame, strategies boosting fuel/air mixing are welcomed. For example, varied number of small fuel ports, their different alignment position or even bluff body introduced into air jet can be tried to explore more rapid mixing and subsequent more controllable combustion. On the other hand, swirl-induced decay of axial flow velocity is another major concern for achieving higher heat transfer rate or efficiency. Newer designs based on CAPs concept fitted with changes to allow weak or ultra-weak swirl will also be appreciated in the future.

As for laminar IDF, CoA IDF burner had been employed in many laboratories around the world for study of the mechanisms responsible for soot formation. The soot formation and oxidation mechanisms were understood by considering particular flow field features of laminar CoA IDF which is suitable for young soot studies. In contrast, though there were some experiments conducted on turbulent CoA IDF soot, but the emphasis is to build and validate soot model or mechanism couple or to be coupled with turbulent combustion models. This review has clarified the flow structure and flame patterns of not only CoA IDF, but also CAPs IDF and swirl IDF. First of all, it would be of great interest to study and compare the sooting characteristics within such family of laminar IDFs. Second, it is desirable by extending these studies from laminar IDFs to turbulent ones, so as to broaden our horizon about interactions between turbulence and soot emission.

Declaration of Competing Interest

We, here, declare that the manuscript captioned has not been simultaneously submitted to other journal for publication consideration and that the work is new based on our own data.

Acknowledgement

The authors thank the National Natural Science Foundation of China (51766003) for financial support of the present study.

References

[1] B.A. Fleck, A. Sobiesiak, H.A. Becker, Experimental and numerical investigation of the novel low NOx CGRI Burner, Combust. Sci. Technol. 161 (1) (2000) 89–112.
[2] W.P. Partridge, J.R. Reisel, N.M. Laurendeau, Laser-saturated fluorescence measurements of nitric oxide in an inverse diffusion flame, Combustion and Flame 116 (1999) 282–290.
[3] B. Stelzner, F. Hunger, A. Laugwitz, M. Gräbner, S. Voss, K. Uebel, et al., Development of an inverse diffusion partial oxidation flame and model burner contributing to the development of 3rd generation coal gasifiers, Fuel Process. Technol. 110 (2013) 33–45.
[4] S.A. Schumaker, J.F. Driscoll, Coaxial turbulent jet flames: scaling relations for measured stoichiometric mixing lengths, Proc. Combust. Inst. 32 (2) (2009) 1655–1662.
[5] A. Sinha, R. Ganguly, I.K. Puri, Control of confined nonpremixed flames using a microjet, Int. J. Heat Fluid Flow 26 (2005) 431–439.
[6] P.B. Sunderland, S.S. Krishnan, J.P. Gore, Effects of oxygen enhancement and gravity on normal and inverse laminar jet diffusion flames, Combustion and Flame 136 (1–2) (2004) 254–256.
[7] A.M. Elbaz, W.L. Roberts, Stability and structure of inverse swirl diffusion flames with weak to strong swirl, Exp. Thermal Fluid Sci. 112 (2020) 109989.
[8] B. Kashir, S. Tabejamaat, N. Jalalatian, On large eddy simulation of blended CH_4–H_2 swirling inverse diffusion flames: the impact of hydrogen concentration on thermal and emission characteristics, Int. J. Hydrog. Energy 40 (45) (2015) 15732–15748.
[9] D.R. Richardson, N. Jiang, D.L. Blunck, J.R. Gord, S. Roy, Characterization of inverse diffusion flames in vitiated cross flows via two-photon planar laser-induced fluorescence of CO and 2-D thermometry, Combustion and Flame 168 (2016) 270–285.
[10] J.N. Friend, The Chemistry of Combustion, Gurney & Jackson, 1922.
[11] L.K. Sze, C.S. Cheung, C.W. Leung, Appearance, temperature, and NO_x emission of two inverse diffusion flames with different port design, Combustion and Flame 144 (1–2) (2006) 237–248.
[12] T. Takagi, Z. Xu, M. Komiyama, Preferential diffusion effects on the temperature in usual and inverse diffusion flames, Combustion and Flame 106 (1996) 252–260.
[13] D. Biswas, A. Mukhopadhyay, Effect of CO_2 and O_2 enhancement and gravity variations on normal and inverse laminar diffusion flames, Materials Today: Proceedings 3 (2016) 3318–3327.
[14] A. Nekkanti, A.L. Sánchez, F.A. Williams, Explanations of influences of differential diffusion on flame-temperature variations in usual and inverse jet flames, Combustion and Flame 200 (2019) 262–264.
[15] Z. Wang, P.B. Sunderland, R.L. Axelbaum, Double blue zones in inverse and normal laminar jet diffusion flames, Combustion and Flame 211 (2020) 253–259.
[16] F. Hunger, M.F. Zulkifli, B.A.O. Williams, F. Beyrau, C. Hasse, Comparative flame structure investigation of normal and inverse turbulent non-premixed oxy-fuel flames using experimentally recorded and numerically predicted Rayleigh and OH-PLIF signals, Proc. Combust. Inst. 36 (2) (2017) 1713–1720.
[17] C. Paladpokkrong, D. Liu, Y. Ying, W. Wang, R. Zhang, Soot reduction by addition of dimethyl carbonate in normal and inverse ethylene diffusion flames: Nanostructural evidence, Journal of Environental Sciences 72 (2018) 107–117.
[18] Y. Ying, D. Liu, Effects of butanol isomers additions on soot nanostructure and reactivity in normal and inverse ethylene diffusion flames, Fuel 205 (2017) 109–129.
[19] X. Zhu, X. Xia, P. Zhang, Near-field flow stability of buoyant methane/air inverse diffusion flames, Combustion and Flame 191 (2018) 66–75.
[20] M. Mikofski, T. Williams, C. Shaddix, L. Blevins, Flame height measurement of laminar inverse diffusion flames, Combustion and Flame 146 (1–2) (2006) 63–72.
[21] J. Miao, C.W. Leung, C.S. Cheung, Effect of hydrogen percentage and air jet Reynolds number on fuel lean flame stability of LPG-fired inverse diffusion flame with hydrogen enrichment, Int. J. Hydrog. Energy 39 (1) (2014) 602–609.
[22] Ł.J. Kapusta, C. Shuang, M. Aldén, Z. Li, Structures of inverse jet flames stabilized on a coaxial burner, Energy 193 (2020) 116757.
[23] A.M. Elbaz, W.L. Roberts, Experimental study of the inverse diffusion flame using high repetition rate OH/acetone PLIF and PIV, Fuel 165 (2016) 447–461.
[24] V. Patel, R. Shah, Experimental investigation on flame appearance and emission characteristics of LPG inverse diffusion flame with swirl, Appl. Therm. Eng. 137 (2018) 377–385.

[25] M.D.L. Cruz-Ávila, E. Martínez-Espinosa, G. Polupan, W. Vicente, Numerical study of the effect of jet velocity on methane-oxygen confined inverse diffusion flame in a 4 Lug-Bolt array, Energy 141 (2017) 1629–1649.
[26] S. Mahesh, D.P. Mishra, Effect of air jet momentum on the topological features of turbulent CNG inverse jet flame, Fuel 241 (2019) 1068–1075.
[27] S. Mahesh, D.P. Mishra, Flame stability and emission characteristics of turbulent LPG IDF in a backstep burner, Fuel 87 (12) (2008) 2614–2619.
[28] S. Mahesh, D.P. Mishra, Flame stability limits and near blowout characteristics of CNG inverse jet flame, Fuel 153 (2015) 267–275.
[29] L.L. Dong, C.S. Cheung, C.W. Leung, Heat transfer characteristics of an impinging inverse diffusion flame jet – part I: Free flame structure, Int. J. Heat Mass Transf. 50 (25–26) (2007) 5108–5123.
[30] H.S. Zhen, C.W. Leung, C.S. Cheung, Thermal and emission characteristics of a turbulent swirling inverse diffusion flame, Int. J. Heat Mass Transf. 53 (5–6) (2010) 902–909.
[31] H.S. Zhen, C.W. Leung, C.S. Cheung, A comparison of the thermal, emission and heat transfer characteristics of swirl-stabilized premixed and inverse diffusion flames, Energy Convers. Manag. 52 (2) (2011) 1263–1271.
[32] A. Kotb, H. Saad, A comparison of the thermal and emission characteristics of co and counter swirl inverse diffusion flames, Int. J. Therm. Sci. 109 (2016) 362–373.
[33] J. Miao, C.W. Leung, C.S. Cheung, Z.H. Huang, H.S. Zhen, Effect of hydrogen addition on overall pollutant emissions of inverse diffusion flame, Energy 104 (2016) 284–294.
[34] Y.S. Choy, H.S. Zhen, C.W. Leung, H.B. Li, Pollutant emission and noise radiation from open and impinging inverse diffusion flames, Appl. Energy 91 (1) (2012) 82–89.
[35] V.R. Katta, L.G. Blevins, W.M. Roquemore, Dynamics of an inverse diffusion flame and its role in polycyclic-aromatic-hydrocarbon and soot formation, Combustion and Flame 142 (1–2) (2005) 33–51.
[36] A. Santamaria, N. Yang, E. Eddings, F. Mondragon, Chemical and morphological characterization of soot and soot precursors generated in an inverse diffusion flame with aromatic and aliphatic fuels, Combustion and Flame 157 (1) (2010) 33–42.
[37] Y. Jung, K.C. Oh, C. Bae, H.D. Shin, The effect of oxygen enrichment on incipient soot particles in inverse diffusion flames, Fuel 102 (2012) 199–207.
[38] M. Velásquez, F. Mondragón, A. Santamaría, Chemical characterization of soot precursors and soot particles produced in hexane and diesel surrogates using an inverse diffusion flame burner, Fuel 104 (2013) 681–690.
[39] F. Escudero, A. Fuentes, R. Demarco, J.L. Consalvi, F. Liu, J.C. Elicer-Cortés, et al., Effects of oxygen index on soot production and temperature in an ethylene inverse diffusion flame, Exp. Thermal Fluid Sci. 73 (2016) 101–108.
[40] Y. Ying, D. Liu, Nanostructure evolution and reactivity of nascent soot from inverse diffusion flames in CO_2, N_2, and he atmospheres, Carbon 139 (2018) 172–180.
[41] G.W. Lee, J. Jurng, J. Hwang, Formation of Ni-catalyzed multiwalled carbon nanotubes and nanofibers on a substrate using an ethylene inverse diffusion flame, Combustion and Flame 139 (1–2) (2004) 167–175.
[42] C.J. Unrau, R.L. Axelbaum, P. Biswas, P. Fraundorf, Synthesis of single-walled carbon nanotubes in oxy-fuel inverse diffusion flames with online diagnostics, Proc. Combust. Inst. 31 (2) (2007) 1865–1872.
[43] S. Li, Y. Ren, P. Biswas, S.D. Tse, Flame aerosol synthesis of nanostructured materials and functional devices: Processing, modeling, and diagnostics, Prog. Energy Combust. Sci. 55 (2016) 1–59.
[44] O. Padilla, J. Gallego, A. Santamaría, Using benzene as growth precursor for the carbon nanostructure synthesis in an inverse diffusion flame reactor, Diam. Relat. Mater. 86 (2018) 128–138.
[45] G. Woo Lee, J. Jurng, J. Hwang, Synthesis of carbon nanotubes on a catalytic metal substrate by using an ethylene inverse diffusion flame, Carbon 42 (3) (2004) 682–685.
[46] L.K. Sze, C.S. Cheung, C.W. Leung, Temperature distribution and heat transfer characteristics of an inverse diffusion flame with circumferentially arranged fuel ports, Int. J. Heat Mass Transf. 47 (14–16) (2004) 3119–3129.
[47] L.L. Dong, C.S. Cheung, C.W. Leung, Heat transfer characteristics of an impinging inverse diffusion flame jet. Part II: Impinging flame structure and impingement heat transfer, Int. J. Heat Mass Transf. 50 (25–26) (2007) 5124–5138.
[48] T.K. Ng, C.W. Leung, C.S. Cheung, Experimental investigation on the heat transfer of an impinging inverse diffusion flame, Int. J. Heat Mass Transf. 50 (17–18) (2007) 3366–3375.
[49] L.L. Dong, C.S. Cheung, C.W. Leung, Characterization of impingement region from an impinging inverse diffusion flame jet, Int. J. Heat Mass Transf. 56 (1–2) (2013) 360–369.
[50] L.L. Dong, C.S. Cheung, C.W. Leung, Heat transfer optimization of an impinging port-array inverse diffusion flame jet, Energy 49 (2013) 182–192.
[51] H.S. Zhen, Y.S. Choy, C.W. Leung, C.S. Cheung, Effects of nozzle length on flame and emission behaviors of multi-fuel-jet inverse diffusion flame burner, Appl. Energy 88 (9) (2011) 2917–2924.
[52] H.S. Zhen, C.S. Cheung, C.W. Leung, H.B. Li, Thermal and heat transfer behaviors of an inverse diffusion flame with induced swirl, Fuel 103 (2013) 212–219.
[53] V. Patel, R. Shah, Effect of hydrogen enrichment on combustion characteristics of methane swirling and non-swirling inverse diffusion flame, Int. J. Hydrog. Energy 44 (52) (2019) 28316–28329.
[54] J. Miao, C.W. Leung, C.S. Cheung, Z. Huang, W. Jin, Effect of H_2 addition on OH distribution of LPG/Air circumferential inverse diffusion flame, Int. J. Hydrog. Energy 41 (22) (2016) 9653–9663.
[55] H.S. Zhen, C.W. Leung, C.S. Cheung, Combustion characteristics of a swirling inverse diffusion flame upon oxygen content variation, Appl. Energy 88 (9) (2011) 2925–2933.
[56] Y.S. Choy, H.S. Zhen, C.W. Leung, C.S. Cheung, R.C.K. Leung, Noise generation by open inverse diffusion flames, J. Vib. Control. 20 (11) (2014) 1671–1681.
[57] B.A. Rabee, The effect of inverse diffusion flame burner-diameter on flame characteristics and emissions, Energy 160 (2018) 1201–1207.
[58] L.G. Blevins, R.A. Fletcher, B.A. Benner, E.B. Steel, G.W. Mulholland, The existence of young soot in the exhaust of inverse diffusion flames, Proc. Combust. Inst. 29 (2002) 2325–2333.
[59] A. Santamaría, F. Mondragón, W. Quiñónez, E.G. Eddings, A.F. Sarofim, Average structural analysis of the extractable material of young soot gathered in an ethylene inverse diffusion flame, Fuel 86 (12–13) (2007) 1908–1917.
[60] A. Santamaria, F. Mondragon, A. Molina, N. Marsh, E. Eddings, A. Sarofim, FT-IR and 1H NMR characterization of the products of an ethylene inverse diffusion flame, Combustion and Flame 146 (1–2) (2006) 52–62.
[61] C.R. Shaddix, T.C. Williams, L.G. Blevins, R.W. Schefer, Flame structure of steady and pulsed sooting inverse jet diffusion flames, Proc. Combust. Inst. 30 (1) (2005) 1501–1508.
[62] S. Mahesh, D.P. Mishra, Flame structure of LPG-air Inverse Diffusion Flame in a backstep burner, Fuel 89 (8) (2010) 2145–2148.
[63] K.T. Wu, R.H. Essenhigh, Mapping and structure of inverse diffusion flames of methane, in: Twentieth Symposium (International) on Combustion/The Combustion Institute, 1984, pp. 1925–1932.
[64] R.F. Huang, Flame and flow characteristics of double concentric jets, Combustion and Flame 108 (1997) 9–23.
[65] A. Sobiesiak, J.C. Wenzell, Characteristics and structure of inverse flames of natural gas, Proc. Combust. Inst. 30 (1) (2005) 743–749.
[66] Y. Bindar, A. Irawan, Size and structure of LPG and hydrogen inverse diffusion flames at high level of fuel excess, Combustion Energy 33 (2002) 124–130.
[67] L.L. Dong, C.S. Cheung, C.W. Leung, Combustion optimization of a port-array inverse diffusion flame jet, Energy 36 (5) (2011) 2834–2846.
[68] H.S. Zhen, C.W. Leung, C.S. Cheung, Heat transfer from a turbulent swirling inverse diffusion flame to a flat surface, Int. J. Heat Mass Transf. 52 (11–12) (2009) 2740–2748.
[69] H.S. Zhen, C.W. Leung, C.S. Cheung, Emission of impinging swirling and non-swirling inverse diffusion flames, Appl. Energy 88 (5) (2011) 1629–1634.
[70] H.S. Zhen, C.W. Leung, C.S. Cheung, Thermal and Emission Characteristics of a Turbulent Inverse Diffusion Flame with Induced High-Swirl, 2008.
[71] R. Ganguly, I.K. Puri, Nonpremixed flame control with microjets, Exp. Fluids 36 (4) (2004) 635–641.
[72] E.M. Clausing, D.W. Senser, N.M. Laurendeau, Peclet correlation for stability of inverse diffusion flames in methane-air cross flows, Combustion and Flame 110 (1997) 405–408.
[73] T. Zhang, Q. Guo, X. Song, Z. Zhou, G. Yu, The chemiluminescence and structure properties of normal/inverse diffusion flames, Journal of Spectroscopy 2013 (2013) 1–7.
[74] M.J. Remie, M.F.G. Cremers, K.R.A.M. Schreel, L.P.H. de Goey, Analysis of the heat transfer of an impinging laminar flame jet, Int. J. Heat Mass Transf. 50 (13–14) (2007) 2816–2827.
[75] P. Liu, H. Jin, B. Chen, et al., Rapid soot inception via α-alkynyl substitution of polycyclic aromatic hydrocarbons, Fuel 295 (2021) 120580.
[76] P. Liu, Z. Li, A. Bennett, et al., The site effect on PAHs formation in HACA-based mass growth process, Combustion and Flame 199 (2019) 54–68.
[77] J. Appel, H. Bockhorn, M. Frenklach, Kinetic modeling of soot formation with detailed chemistry and physics: laminar premixed flames of C2 hydrocarbons, Combustion and flame 121 (1–2) (2000) 122–136.
[78] H.A. Michelsen, Probing soot formation, chemical and physical evolution, and oxidation: a review of in situ diagnostic techniques and needs, Proc. Combust. Inst. 36 (1) (2017) 717–735.
[79] A.E. Karataş, Ö.L. Gülder, Soot formation in high pressure laminar diffusion flames, Prog. Energy Combust. Sci. 38 (6) (2012) 818–845.
[80] H. Richter, J.B. Howard, Formation of polycyclic aromatic hydrocarbons and their growth to soot - a review of chemical reaction pathways, Prog. Energy Combust. Sci. 26 (2000) (656–08).
[81] A. Gomez, M.G. Littman, I. Glassman, Comparative study of soot formation on the centerline of axisymmetric laminar diffusion flames fuel and temperature effects, Combustion Flame 70 (2) (1987) 225–241.
[82] P. Liu, B. Chen, Z. Li, et al., Experimental and theoretical evidence for the temperature-determined evolution of PAH functional groups, Proc. Combust. Inst. 38 (1) (2021) 1467–1475.
[83] K.T. Kang, J.Y. Hwang, S.H. Chung, Soot zone structure and sooting limit in diffusion flames comparison of counterflow and co-flow flames, Combustion and Flame 109 (1997) 266–281.
[84] C.R. Kaplan, K. Kailasanath, Flow-field effects on soot formation in normal and inverse methane-air diffusion flames, Combustion and Flame 124 (2001) 275–294.
[85] E. Lee, K. Oh, H. Shin, Soot formation in inverse diffusion flames of diluted ethene, Fuel 84 (5) (2005) 543–550.
[86] Y. Wang, S.H. Chung, Strain rate effect on sooting characteristics in laminar counterflow diffusion flames, Combustion and Flame 165 (2016) 433–444.
[87] K. Oh, U. Lee, H. Shin, E. Lee, The evolution of incipient soot particles in an inverse diffusion flame of ethene, Combustion and Flame 140 (3) (2005) 249–254.

[88] C.R. Shaddix, T.C. Williams, Measurements of the velocity field in laminar ethylene inverse jet diffusion flames, Combustion and Flame 156 (4) (2009) 942–945.
[89] B.M. Kumfer, S.A. Skeen, R.L. Axelbaum, Soot inception limits in laminar diffusion flames with application to oxy–fuel combustion, Combustion and Flame 154 (3) (2008) 546–556.
[90] M. Wei, J. Liu, G. Guo, S. Li, The effects of hydrogen addition on soot particle size distribution functions in laminar premixed flame, Int. J. Hydrog. Energy 41 (14) (2016) 6162–6169.
[91] M. Gu, H. Chu, F. Liu, Effects of simultaneous hydrogen enrichment and carbon dioxide dilution of fuel on soot formation in an axisymmetric coflow laminar ethylene/air diffusion flame, Combustion and Flame 166 (2016) 216–228.
[92] Y. Ying, C. Xu, D. Liu, B. Jiang, P. Wang, W. Wang, Nanostructure and Oxidation Reactivity of Nascent Soot Particles in Ethylene/Pentanol Flames, Energies 10 (1) (2017) 122.
[96] B.F. Magnussen, B.H. Hjertager, J.G. Olsen, D. Bhaduri, Effects of turbulent structure and local concentrations on soot formation and combustion in C_2H_2 diffusion flames, Symp. Combust. 17 (1979) 1383–1393.
[97] B.F. Magnussen, An investigation into the behavior of soot in a turbulent free jet C2H2-flame, Symp. Combust. 15 (1975) 1415–1425.
[98] B.F. Magnussen, B.H. Hjertager, On mathematical modeling of turbulent combustion with special emphasis on soot formation and combustion, Symp. Combust. 16 (1977) 719–729.
[99] Y. Wang, S.H. Chung, Soot formation in laminar counterflow flames, Prog. Energy Combust. Sci. 74 (2019) 152–238.
[100] F. Bisetti, G. Blanquart, M.E. Mueller, H. Pitsch, On the formation and early evolution of soot in turbulent nonpremixed flames, Combustion and Flame 159 (1) (2012) 317–335.
[101] M. Yamamoto, S. Duan, S. Senkan, The effect of strain rate on polycyclic aromatic hydrocarbon (PAH) formation in acetylene diffusion flames, Combustion and Flame 151 (3) (2007) 532–541.
[102] B. Hu, U. Koylu, Size and morphology of soot particulates sampled from a turbulent nonpremixed acetylene flame, Aerosol Sci. Technol. 38 (10) (2004) 1009–1018.
[103] A.M. Elbaz, W.L. Roberts, Flame structure of methane inverse diffusion flame, Exp. Thermal Fluid Sci. 56 (2014) 23–32.
B. Jiang, P. Wang, Y. Ying, M. Luo, D. Liu, Nanoscale characteristics and reactivity of nascent soot from n-heptane/2,5-dimethylfuran inverse diffusion flames with/without magnetic fields, Energies 11 (7) (2018) 1698.
P. Jia, D. Liu, Y. Ying, M. Luo, B. Jiang, R. Zhang, Nanostructure and reactivity of nascent carbon particles from 2,5-dimethylfuran/n-heptane swirling inverse diffusion flames, Fullerenes, Nanotubes and Carbon Nanostructures 27 (2) (2019) 106–119.
R. Demarco, J.-L. Consalvi, A. Fuentes, A calibrated soot production model for ethylene inverse diffusion flames at different Oxygen indexes, Fuel 212 (2018) 1–11.